SOM Text: Supplemental Information and Discussion

Analysis of genomic instability in disome IV: We noted that disome IV apparently displays lower levels of genomic instability than wild-type in three different assays (chromosome loss, forward mutation, and microsatellite instability) that use FOA-based selection. These results stand in contrast to our observations that disome IV has an increased mutation rate at *CAN1* (Fig. 2A), is sensitive to benomyl (Fig. 1B), and displays persistent Rad52-GFP foci (Fig. 3A). Disome IV has the worst proliferative capacity of the 13 disomic strains; it has a doubling time of 6-8 hours and very low plating efficiency (*1*). We believe that disome IV may exhibit FOA hypersensitivity which interferes with our ability to measure genomic instability in this strain using FOA-based assays. We note that disome IV exhibits elevated levels of ribonucleotide reductase (*1*), and RNR over-expression has been linked to FOA hypersensitivity (*2*). Nevertheless, results obtained with other assays confirm that disome IV displays heightened genomic instability.

Chromosome segregation analysis and experimental rationale: The increased rate of YAC loss (Fig. 1A) and benomyl sensitivity (Fig. 1B) in disomic strains demonstrates that aneuploidy interferes with accurate chromosome segregation. We note, however, that not all strains displaying YAC loss are benomyl sensitive, and vice-versa. Strains which are sensitive to benomyl but do not display heightened YAC loss may be defective in chromosome segregation in the presence of spindle damage but not during an unperturbed cell cycle. Alternately, strains which are benomyl resistant but frequently missegregate a YAC may predominantly have defects in microtubule-independent DNA replication and repair processes.

In 5 out of 5 disomic strains, we observed prolonged Pds1 persistence, demonstrating a cell cycle delay prior to anaphase (Figs. 1C and S1). Deletion of *MAD2* suppressed this persistence in disome V, but not in four other disomes, suggesting that disome V has a chromosome alignment defect which triggers a Mad2-dependent checkpoint (Fig. 1C and S1). In order to confirm this hypothesis, we arrested disomes V and XVI in mitosis with nocodazole and then examined the kinetics of Pds1 degradation following release from the block (Fig. S2). This assay is especially sensitive in detecting bi-orientation defects, because cells have to reestablish bi-orientation of all sister chromatids following drug removal. This analysis confirmed a bi-orientation defect in disome V cells. Following the removal of nocodazole, disome XVI and wild-type strains rapidly degraded Pds1, while a degradation delay was apparent in disome V cells (Fig. S2). We conclude that in most disomes the stabilization of Pds1 and increase in chromosome loss result predominantly from Mad2-independent defects in genome replication and repair, while in disome V cells problems in sister kinetochore bi-orientation elicit a Mad2-dependent cell cycle delay.

Mutation spectra in aneuploid and wild-type strains: In order to define the molecular mechanism underlying the increased mutation rate in aneuploid cells, we sequenced the *CAN1* allele from 133 wild-type and 404 disomic canavanine-resistant isolates (Table S1). Disomic sequences included 24 to 32 *CAN1* alleles from 10 different disomes, 73 alleles from disome X (a mutator), and 79 alleles from disome IX (a non-mutator). In order to make statistically-significant comparisons with the wild-type strain, the pooled total of all aneuploid *CAN1* alleles was initially considered. Significant differences were determined using the chi-square goodness-of-fit test. In addition to the increase in complex events discussed in the main text, we also observed that the identity of basepairs gained and lost in the disomes differed relative to wild-

type in a largely strand-specific manner. For example, 11 out of 12 disomes displayed an increased frequency of substitution to adenine on the coding strand while 9 out of 12 disomes displayed a decreased frequency of substitution to adenine on the non-coding strand (Table S2). Mutation to adenine occurs preferentially opposite damaged bases, suggesting the presence of unrepaired lesions on the non-coding strand (*3*). This alteration in spectrum is also apparent when specific mutation events (i.e. CG>TA substitutions) are scored with respect to a particular strand, but there is no significant difference in CG>TA substitution frequency when events are scored independently of strand identity (Table S3 and S4). The only strand-independent alteration in substitution frequency is an increase in AT>TA transversions in the disomes (Table S4). Additionally, we analyzed sequence differences between the pooled total of all mutator strains (Dis. IV, VIII, X, and XIV) and the wild-type population. The decreased number of alleles considered diminished the statistical power of our tests, and some differences apparent among the pooled total of all aneuploid strains (i.e., increased substitution to adenine on the coding strand) were no longer significant. However, mutator disomes did exhibit a strand-independent decrease in CG>AT substitutions that was not present among all aneuploid alleles. Note that this is a potentially biased comparison, as disome X constitutes greater than 50% of the basepair substitutions in mutator strains and removing disome X abolishes the apparent difference. The cause of these basepair substitution frequency alterations is at present unknown.

Double-strand break formation and repair in the disomes: A common phenotype among the disomic strains is severe sensitivity to phleomycin and bleomycin, two double-strand break inducing drugs (Fig. 2C). Indeed, the sensitivity of disomes IV, VIII, X, XI, and XIV to these drugs was comparable to the sensitivity of a strain lacking Rad51. Corroborating this observation, we found that many disomes display an increased number of Rad52-GFP foci (Fig.

3A) and a moderate hyper-recombination phenotype (Fig. 3C). Two non-mutually exclusive models could account for these observations. First, disomes could accumulate more DSBs than euploid cells do, either during a normal cell cycle or upon treatment with phleomycin. Secondly, regardless of the number of DSBs which are formed, the disomes could repair the DSBs more slowly than wild-type and/or incorrectly. Our analysis of *rad52*Δ disomes suggests that disomes XI, XII, and XIV accumulate more DSB's during DNA replication, while disomes VIII and XV do not (Fig. S6). Pulse-field gel analysis of several disomes treated with phleomycin is consistent with a defect in DSB repair, though it could also be explained by defects in DNA damage avoidance: chromatin in disomes may be more vulnerable than euploid chromatin to phleomycin-induced lesions (Fig. 3D and S9). However, we believe that a drug efflux problem is unlikely to account for any differences in phleomycin sensitivity, as the disomes are also sensitive to UV light (Fig. 2B). We further note that a DSB-repair defect is not inconsistent with our finding that disomes are moderately hyper-recombinant, as many mutations in genes which compromise DNA repair also display increased mitotic recombination [i.e., *ELG1* (*4*), *RTT109* (*5*), and *SGS1* (*6*)].

Causes of aneuploidy-induced genomic instability: We have demonstrated that replication of an extra chromosome *per se* is not sufficient to impair recombination or DNA damage resistance, but that it is likely that stoichiometric imbalances in yeast proteins cause genomic instability (Fig. 4). However, aneuploidy-induced genomic instability is uncorrelated with the size of the extra chromosome (Fig. S12). This may suggest that genomic instability is caused by imbalances in a few specific genes which are randomly distributed throughout the genome. For instance, altering the stoichiometry of histones and spindle pole proteins has been shown to interfere with accurate chromosome segregation (*7*-*9*). Alternately, proteotoxic stress caused by

the translation, folding, and degradation of many proteins on the extra chromosomes (*1, 10*) could contribute to genomic instability. Aneuploidy may monopolize cellular chaperones and protein turnover complexes, thereby inhibiting the function of other proteins that normally require their use. Distinguishing between these possibilities will be an important aspect of our future studies.

Material and Methods

Strains and Plasmids: All budding yeast strains used in this study are derivates of W303 (A2587/A2588) and are listed in Tables S6 and S7. Strains were constructed using PCR-based methods for gene deletion and tagging (*11*). The generation of aneuploid strains has been previously described (*1*). All aneuploid strains were analyzed by comparative genomic hybridization (CGH) to ensure that the specified extra chromosome was present in its entirety (*1*). YACs used in this study are listed in Table S8 (*12, 13*).

Analysis of genotoxin sensitivities: For each assay, fresh plates were prepared containing the concentrations of genotoxins indicated in the figures. Plates containing phleomycin and camptothecin were buffered with 50mM HEPES (pH 7.4). For each assay, strains were inoculated O/N in appropriate selective media, then 10-fold serial dilutions were prepared in sterile water and spotted onto plates. Camptothecin and UV-treated plates were incubated in the dark. In Fig. 1B, the following strains were used: A11311, A24694, A12683, A12685, A12687, A14479, A13628, A13975, A21986, A13771, A12693, A21987, A13979, A12697, and A12700. In Fig. 2B and 2C, the following strains were used: A11311, A21598, A12683, A12685, A12687, A14479, A13628, A13975, A21986, A13771, A12693, A21987, A13979, A12697, and A12700. In Fig. 3E, the following strains were used: HM123, P219, and P523. In Fig. 4A, the

following strains were used: A11311, A13628, A17392, A17393, A17394, A17395, A17396, and A23744. In Fig. 4D, the following strains were used: A11311, A18344, A14479, A18346, A13628, A18347, A12693, A19549, A13979, A18349, A12697, and A18350.

Determination of Chromosome Loss Rates: The rate of chromosome loss was calculated as previously described (*14*). YAC yWSS1572, which is marked with *TRP1* and *URA3* at opposing telomeres, was crossed into the strains of interest (*12*). Strains were first inoculated O/N in –HIS-TRP-URA+G418 medium. Subsequently, ~1000 cells were transferred to 2ml of –HIS+G418 medium, and appropriate dilutions were plated onto –HIS+G418 and –HIS+G418 supplemented with 1mg/ml 5-fluoroorotic acid (FOA) to determine the fraction of cells which had lost the YAC prior to the start of the assay. Cells were allowed to divide for 24-36 hours, then were diluted and plated on –HIS+G418 and –HIS+G418+FOA. For chromosome loss experiments in diploid and trisomic strains, cells were pre-grown in –HIS-LEU-URA-TRP+G418 medium, transferred to –HIS-LEU+G418 medium, then plated on either –HIS-LEU+G418 or –HIS-LEU+G418+FOA. The number of cells that maintained the chromosome during the assay was calculated using the formula $S = F(1-m)$, where F is the total number of cells and m is the fraction of cells which lost the chromosome during the assay. The chromosome loss rate per generation was calculated using the formula $L = 1 - \frac{(\frac{S}{C})^{\frac{1}{N}}}{2}$, where C is the number of cells initially inoculated and N is the number of generations that the culture grew. Cell numbers for plating were determined using a Beckman Coulter Multisizer 3. For 6 cultures from each strain, colonies that grew on FOA plates were replica plated to –TRP plates to control for mutation or loss of a single chromosome arm. On average, >97% of FOA^R colonies were also Trp-, demonstrating that whole-chromosome loss was almost always the cause of FOA

resistance. Chromosome loss rates are presented as the mean and standard deviation of at least 12 independent cultures. In Fig. 1A, the following strains were used: A23744, A24792, A24660, A23745, A25827, A25340, A23747, A23748, A23749, A25587, A23750, A23751, A25341, A23752, A23753, and A25627. In Fig. 4E, the following strains were used: A27889, A27890, A27891, and A27892. In Fig. 4F, the following strains were used: A23744, A27889, A23750, A27890, A25341, A27891, A23753, and A27892. Note that the data for YAC loss rates in disomic strains is presented in Fig. 1A.

Cell cycle analyses of Pds1 levels and spindle morphology: Cells were inoculated into –HIS +G418 medium and grown to log phase. The cells were subsequently collected by filtration and resuspended at an OD_{600} of 0.175 in YPD medium containing 5 μg/ml α-factor to arrest the cells in G1. 2.5 μg/ml α-factor was re-added every 75 minutes to maintain cells in the G1 arrest. When both the WT and disomic strains were arrested, cells were washed by filtration with 8 volumes of YPD, and the cells were resuspended in fresh YPD medium lacking pheromone. Samples were taken at the indicated time points, and α-factor (5 μg/ml) was readded when more than 50 percent of the cells had formed a bud to prevent cells from entering the next cell cycle. To account for variability between experiments, a wild-type control culture was always analyzed concomitantly with the disomic strains. In Fig. 1C, strains A26703 and A26628 were used.

Western blot analyses: Proteins were extracted from aliquots taken at the indicated time points by adding an equal volume of 10% trichloroacetic acid to the cell culture. The samples were incubated on ice for at least 20 minutes, then washed with 1.5ml of acetone. The dried pellet was resuspended in 100 μL of protein breakage buffer (50mM Tris, pH 7.5, 1mM EDTA, 2.75 mM DTT, and Roche Complete protease inhibitor, used per the manufacturer's instructions). 100 μL of glass beads were added and the cells broken by beating for 2.5 minutes on a Biospec

mini-bead beater. 50 μL of 3X SDS sample buffer was added, the samples boiled for 5 minutes, then centrifuged for 5 minutes. An equal volume of lysate was loaded onto 10% SDS polyacrylamide gel, electrophoresed, and transferred to a nitrocellulose membrane. Pds1-3HA was detected using a mouse anti-HA antibody (HA.11, Covance) at a 1:1,000 dilution. Pgk1 was detected using a mouse anti-Pgk1 antibody (A-6457, Molecular Probes) at a 1:5,000 dilution. The secondary antibody was a sheep anti-mouse antibody coupled to horseradish peroxidase (NA931, GE Healthcare) and used at a 1:5,000 dilution. Rad53 was detected using a goat polyclonal antibody (yC-19, Santa Cruz Biotechnology) at a 1:5,000 dilution, followed by donkey anti-goat antibody coupled to horseradish peroxidase (sc2020, Santa Cruz Biotechnology) at a 1:10,000 dilution. Bands were detected using Pierce SuperSignal West Pico Chemiluminescent Substrate according to the manufacturer's instructions.

Fixation and immunofluorescence of yeast cells: Mitotic spindles were visualized as previously described (*15*), with the following modifications. At each time point, one ml of cell culture was collected and fixed in 3.7% formaldehyde in 0.1 M potassium phosphate buffer. After digestion for 60 minutes with glusulase and zymolyase, cells were applied to polylysine-coated multiwall slides and fixed for 3 minutes in methanol followed by 10 seconds in acetone, both at -20^{o}C. Rat anti-tubulin antibodies (Oxford Biotechnology) and anti-rat FITC antibodies (Jackson Immunoresearch) were used at a 1:100 dilution for visualization of spindle morphology. At least 200 cells were counted per strain for each time point.

Fluctuation analysis: To determine the mutation rate at *CAN1*, ~1000 canavanine-sensitive cells were inoculated in 5ml of –HIS+G418 medium and grown to saturation. Appropriate dilutions were then plated on –HIS+G418 and on -HIS-ARG+G418 medium supplemented with 60μg/ml canavanine to determine the number of viable cells and canavanine-resistant cells, respectively.

The rate of spontaneous mutation was determined according to the method of the median (*16, 17*). Reported mutation rates for each strain are the median values of at least 12 independent cultures. Cell numbers for plating were determined using a Beckman Coulter Multisizer 3. In Fig. 2A, the following strains were used: A20814, A27898, A21630, A25328, A25329, A25330, A25331, A25332, A25333, A25334, A25335, A25336, A25337, A25338, and A25339. To determine the mutation rate at *URA3*, an identical protocol was followed, and cells were plated on –HIS +G418+FOA. In Fig. 2A, the following strains were used: A25589, A25590, A25591, A25592, and A25593. In Fig. 4B, the following strains were used: A20814, A25331, A26980, A26981, and A27683.

The *CAN1* gene is located on chromosome V, and mutations conferring canavanine resistance are recessive. Therefore, to calculate the rate of mutation of a strain disomic for chromosome V, fluctuation analysis was performed for mutation at *LYP1*, which is located on chromosome XIV and confers sensitivity to thialysine (*18*). –HIS-LYS+G418 plates supplemented with 100μg/ml thialysine were used to determine the fraction of thialysine-resistant cells, and the mutation rate was calculated as described above. For this analysis in Fig. 2A, the following strains were used: A24351and A14479.

To determine the rate of mitotic recombination, we used a construct in which a 5'-truncated and a 3'-truncated allele of *ade2* are separated by *URA3* (*19*). ~100 Ura+ cells were inoculated into 5ml of –HIS+G418 medium and grown to saturation. Mitotic recombination was measured by plating on –HIS+G418+FOA to determine the fraction of cells which lost the intervening *URA3* sequence. The rate of mitotic recombination was calculated using the method of the median as above. In Fig. 3C, the following strains were used: A26461, A26473, A26475,

A26462, A26463, A26464, A26465, A26466, A26467, A26468, A26469, A26470, A26471, and A26472.

To determine the rate of microsatellite instability, a plasmid containing *TRP1* and a 16.5-poly(GT) sequence in-frame with *URA3* was crossed into the disomes (*20*). ~100 URA+ cells were inoculated into 5ml of medium and grown to saturation. The fraction of cells that maintained the plasmid was calculated by plating on –HIS-TRP+G418, and the fraction of plasmid-maintaining cells in which *URA3* was out of frame was calculated by plating on –HIS-TRP+G418+FOA. The rate of microsatellite instability was determined using the method of the median as above.

***CAN1* sequencing:** DNA from canavanine-resistant colonies was purified by phenol-chloroform extraction (*21*). The *CAN1* locus was amplified using primers 5'-TCTTCAGACTTCTTAACTCC-3' and 5'-ATAGTAAGCTCATTGATCCC-3'. Sequencing was performed using the following primers (*22*): 5'- AAAAAAGGCATAGCAATGAC-3', 5'-GACGTACAAAGTTCCACTGG-3', 5'- TCAAAGAACAAGTTGGCTCC-3', 5'-TAGATGTCTCCATGTAAGCC-3', 5'- AACTTTGATGGAAGCGACCC-3', and 5'-GAAATGGCGGGGAAATGTG-3'.

Rad52-GFP foci analysis and live cell microscopy: To follow the distribution of Rad52-GFP foci during the cell cycle, cells were arrested in G1 with 10 μg/ml α-factor for 120-180 minutes, then washed and released into –HIS+G418 medium lacking pheromone. Samples were removed every 30-45 minutes to determine the fraction of cells with Rad52-GFP foci. To arrest cells in mitosis, cells were treated with 15 μg/ml nocodazole for 90 minutes. In Fig. 3A, strains used for this assay were as follows: A24352, A26532, A26533, A25342, A25343, A25421, A25344, and

A25345. In Fig. 4C, strains used for this assay were as follows: A24352, A25342, A26985, A26986, and A27667.

To determine whether Rad52-GFP foci appear in other types of aneuploid yeast strains, we created diploid and triploid strains homozygous for the gene encoding the Rad52-GFP fusion protein. Cells were sporulated, then tetrads were dissected on YPD plates. Visible colonies which formed from euploid or aneuploid spores were inoculated in YPD for 3-4 hours, then the frequency of Rad52-GFP foci appearance was scored among budded cells. We note that the actual incidence of Rad52-GFP foci appearance may be even greater among all progeny of triploid meiosis, as spores which form the most foci are unlikely to grow into visible colonies. In Fig. 3B, strains used were A28502 and A27997.

To follow the repair of phleomycin-induced double-strand breaks, cells were arrested in G1 as described above and then released into medium containing 0.15μg/ml phleomycin and buffered with 50mM HEPES (pH 7.4). After 135 minutes, cells were washed twice and transferred to fresh medium. Cells were removed every 30 minutes to score the fraction of large-budded cells and cells containing Rad52-GFP foci.

IR experiments were performed with a Gammacell 40, which uses ^{137}Cesium as a radiation source. Exponentially-growing cultures were treated with 4.5krads to induce double-strand breaks, then samples were removed every 60 minutes to determine the fraction of large-budded cells and cells containing Rad52-GFP foci.

Microscopy was performed using a Zeiss Axioplan 2 microscope with a Hamamatsu OCRA-ER digital camera. Image analysis was performed with Openlab 4.0.2 software.

Pulsed Field Gel Electrophoresis: To directly visualize chromosome damage and repair following phleomycin treatment, yeast cultures were grown overnight in –HIS+G418 medium to log phase. Cells were then harvested and resuspended in fresh YPD medium buffered with 50mM HEPES (pH 7.4) at an OD_{600} of 0.3. Phleomycin was added to a final concentration of 25μg/mL. After two hours, cells were washed with 5 volumes of fresh HEPES buffered YPD and resuspended in HEPES buffered YPD containing 15 μg/ml nocodazole to arrest cells at mitosis to prevent further cell division.

50 ml cell culture aliquots were collected and fixed with sodium azide just prior to the addition of phleomycin (pre), at the end of phleomycin treatment (time 0), and at the indicated timepoints during recovery in YPD medium containing nocodazole. Cell density was determined with a Beckman Coulter Multisizer 3 before and after phleomycin treatment. This allowed us to adjust for cell number increase during drug treatment when making the DNA agarose plug for the "pre" sample, such that the number of cells loaded on the gel was equivalent for the "pre" and the subsequent time points.

Yeast DNA agarose plugs were prepared and processed as described (*23*) by embedding cells in low melting point agarose to a final concentration of 0.625% agarose. The "pre" sample plug was embedded in a smaller volume such that the concentration of cells in the agarose plug would equal that of the others.

Plugs were melted and equal volumes loaded on a 1% agarose gel. DNA was electrophoresed using a Bio-Rad CHEF-DR II system at 6 V/cm at 14ºC. The switch time was 60s for 15 hours followed by 90s for 9 hours. The gel was stained with ethidium bromide and imaged using a GE ImageQuant LAS 4000. In all the images, the wild-type strain was both collected and run concurrently with the disomic strain(s) shown on the same gel. Because

multiple disomic strains were collected during an experiment, some of the final gel images were spliced in order to place the wild-type results next to the disomic strain. No modifications exist in exposure time, contrast, etc. of these spliced images so that the wild-type and disomic strain are directly comparable. In Fig. 3D, the following strains were used: A11311 and A13771.

***Schizosaccharomyces pombe* Genetics and Microscopy:** Strains of fission yeast used in this study are listed in Table S9. The construction of P219, a strain disomic for chromosome III, was previously described (*24*). A triploid strain for sporulation was created by crossing P321 with the mating-competent diploid P322. The products of a triploid meiosis include various combinations of disomy as well as haploid and diploid cells. Strains disomic for chromosome I and/or II arrest before forming a full-size colony, or undergo an unequal nuclear division that results in euploid progeny (*25*). Aneuploid cells can be easily identified during the microcolony stage due to their delayed germ tube formation and aberrant colony morphology.

To analyze the frequency of SpRad22 foci in aneuploid and euploid cells, spores from a triploid meiosis were transferred to YEA medium and incubated at 30ºC. Spores that had germinated and undergone multiple rounds of cell division within 25.5 hours after transfer to YEA were identified as euploid and the frequency of SpRad22 foci was determined. Spores that showed delayed germination and aberrant colony morphology after 48 hours on YEA were identified as aneuploid and the frequency of SpRad22 foci was determined as above.

For time-lapse observations of SpRad22 foci formation, spores from a triploid meiosis were transferred to YEA medium and incubated at 30ºC. Spores that had germinated within 8 hours were identified as euploid and were transferred to a cover slip. Images were acquired every 30 minutes to follow cell division and SpRad22 foci formation. Spores that had

germinated but not divided by 17.5 hours were identified as aneuploid and were followed via microscopy as described above.

DNA sample preparation and microarrays: For the CGH analyses described in Figures S13 and S14, cells were patched from glycerol stocks on YEPD plates. As soon as cells had started to grow, 5 ml cultures were inoculated and grown overnight at room temperature in YEPD. Cells were collected the next day and resuspended into 0.5 ml of 1 M Sorbitol, 10 mM NaPi (pH 7.0), 10 mM EDTA (pH 8.0), 5 µl ß-mercaptoethanol and 20 µl of a 5 mg/ml stock solution of zymolyase. Cell walls were digested by incubation at 37^{o}C for 60 minutes. After a short spin, the supernatant was removed and cells were resuspended in 0.5 ml 50 mM EDTA (pH 8.0), 0.3% SDS, and 20 µg/ml proteinase K and incubated at 65^{o}C for 30 minutes. 200 µl of 5 M KOAc was added and cells were incubated on ice for 20 minutes. Cell debris was removed by centrifugation and supernatant was extracted with an equal volume of phenol/chloroform. DNA samples were recovered by isopropanol precipitation. Precipitated samples were resuspended in 125 µl of TE containing 10 µg/ml RNAse and incubated at 37 ºC for 1 hour. DNA samples were sheared by sonication and further purified utilizing the Qiagen PCR purification kit.

DNA was then labeled with Cy-dye dUTP as described in (*1*). Equal amounts of Cy5-labeled DNA of aneuploid strains were mixed with Cy3-labeled WT DNA and hybridized to the Agilent Yeast Oligo Microarray (V2; Design ID 013384). Arrays were washed following the manufacturer's instructions and scanned with an Agilent Microarray scanner. Data were analyzed using the Agilent Feature extraction software.

DNA copy number analysis: For the CGH analyses described in Figures S13 and S14, $\log_2$ ratios of the gene copy number of the aneuploid strains relative to WT were first obtained

utilizing the normalization protocols of Agilent Feature Extraction software. Data were re-normalized to the mean of $\log_2$ ratio of the euploid chromosomes within each sample. In strain A12, which shows a heterogeneous karyotype, chromosomes VI and XIII were assumed to be the euploid chromosomes as they show the lowest $\log_2$ ratios.

Figure S1

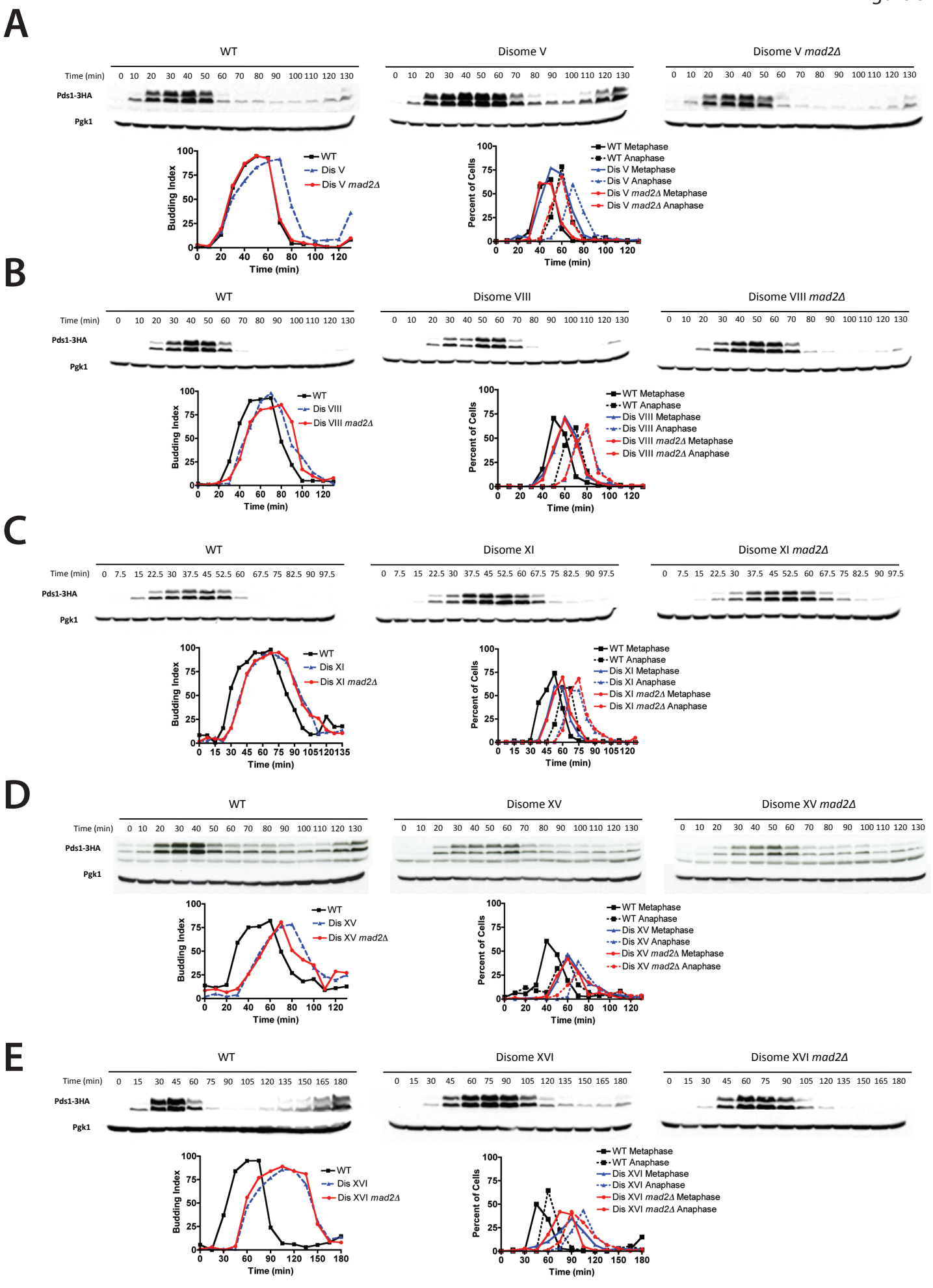
A
WT
Disome V
Disome V mad2Δ
Time (min)
Pds1-3HA
Pgk1
Budding Index
Dis V
Dis V mad2Δ
Percent of Cells
WT Metaphase
WT Anaphase
Dis V Metaphase
Dis V Anaphase
Dis V mad2Δ Metaphase
Dis V mad2Δ Anaphase
B
WT
Disome VIII
Disome VIII mad2Δ
Dis VIII
Dis VIII mad2Δ
Dis VIII Metaphase
Dis VIII Anaphase
Dis VIII mad2Δ Metaphase
Dis VIII Anaphase
C
WT
Disome XI
Disome XI mad2Δ
Dis XI
Dis XI mad2Δ
Dis XI Metaphase
Dis XI Anaphase
Dis XI mad2Δ Metaphase
Dis XI mad2Δ Anaphase
D
WT
Disome XV
Disome XV mad2Δ
Dis XV
Dis XV mad2Δ
Dis XV Metaphase
Dis XV Anaphase
Dis XV mad2Δ Metaphase
Dis XV mad2Δ Anaphase
E
WT
Disome XVI
Disome XVI mad2Δ
Dis XVI
Dis XVI mad2Δ
Dis XVI Metaphase
Dis XVI Anaphase
Dis XVI mad2Δ Metaphase
Dis XVI mad2Δ Anaphase
Time (min)

Figure S1. Pds1 accumulates in disomic strains. Wild-type (squares), disomic strains (triangles), and disomic strains lacking *MAD2* (circles) were arrested in G1 with pheromone then released into YPD medium. At the indicated time points, samples were removed and processed for Western blot analysis of Pds1, to determine the percentage of cells with buds (left graph), and metaphase and anaphase spindles (right graph). In five out of five disomes, Pds1 persisted for a longer period of time than it did in a euploid strain. In disome V cells this delay was due to activation of the spindle assembly check-point because it was eliminated by the deletion of *MAD2*. Strains are as follows: **(A)** A26703, A25413, and AA26708. **(B)** A26703, A25414, and A26709. **(C)** A26703, A25415, and A26704. **(D)** A26703, A26628, and A27925. **(E)** A26703, and A25416, A26705.

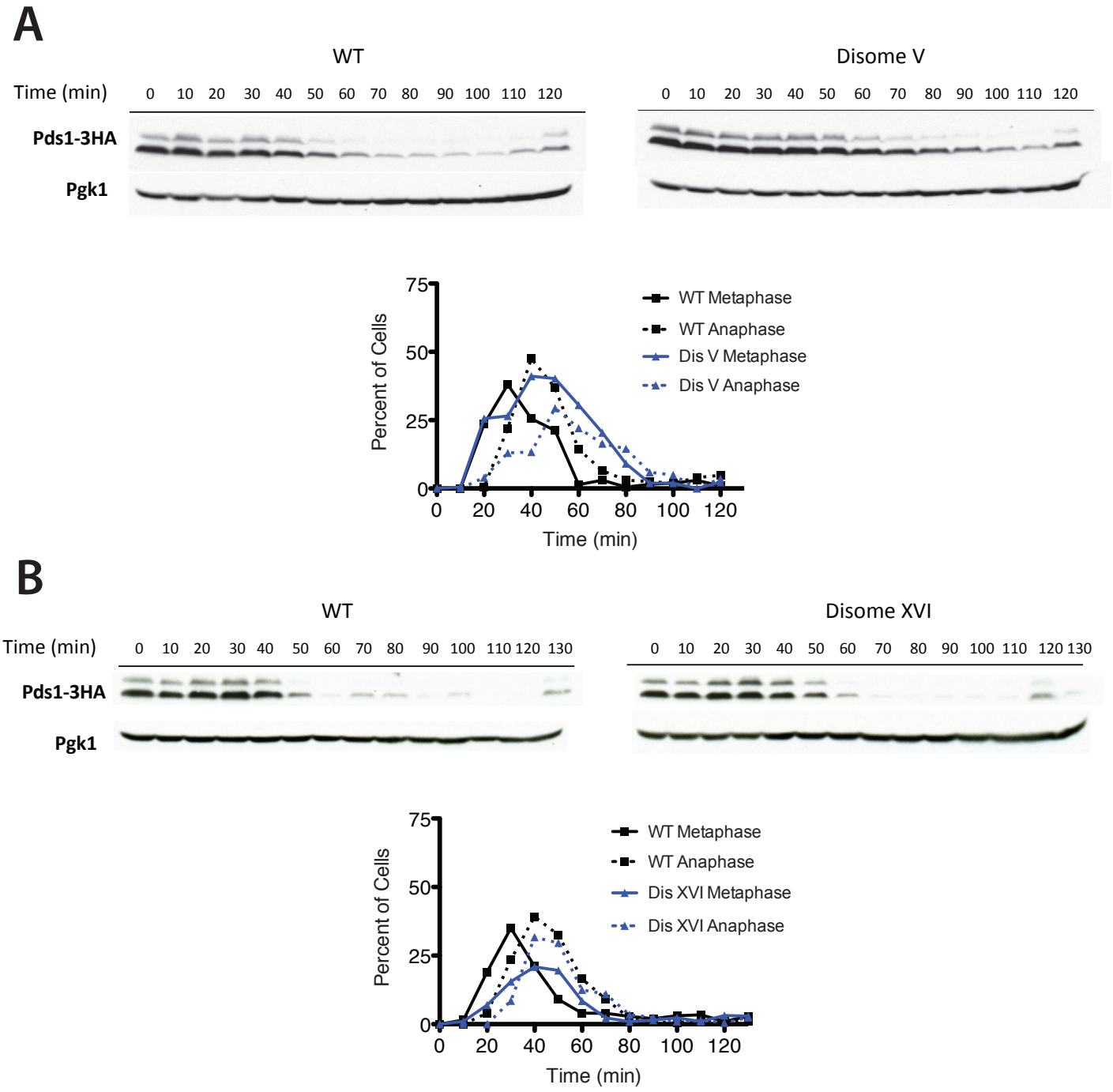

Figure S2. Disome V cells exhibit a chromosome bi-orientation defect. Wild-type and disomic strains were arrested at metaphase with 15 µg/ml nocodazole, then washed and released into YPD medium containing 5 µg/ml α-factor. At the indicated time points, samples were removed and processed for Western blot analysis of Pds1 and to determine the percentage of metaphase (squares) and anaphase (triangles) spindles. Strains are as follows: (**A)** A26703 and A25413. **(B)** A26703 and A25416.

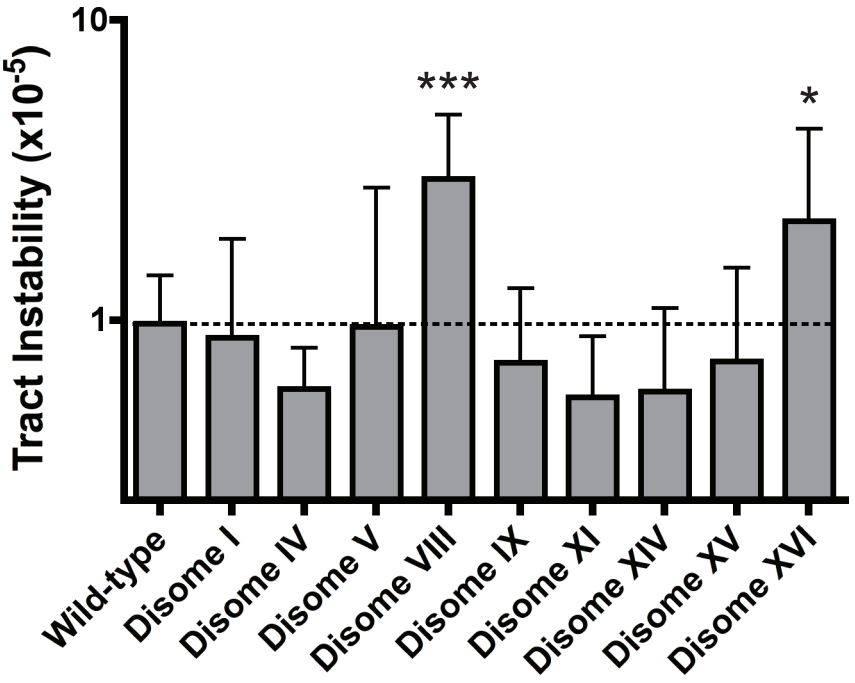

Figure S3. Disomes VIII and XVI cells display an increased rate of microsatellite instability. Disomes were assayed for maintenance of a poly(GT) tract fused in-frame with *URA3*. The median value and 95% confidence intervals of at least 12 independent cultures are shown. Strains (from the left): A24251, A24289, A26498, A24287, A24288, A26499, A26500, A24290, A24291, and A26501. * $p<.05$; *** $p<.0005$ (Wilcoxon rank-sum test).

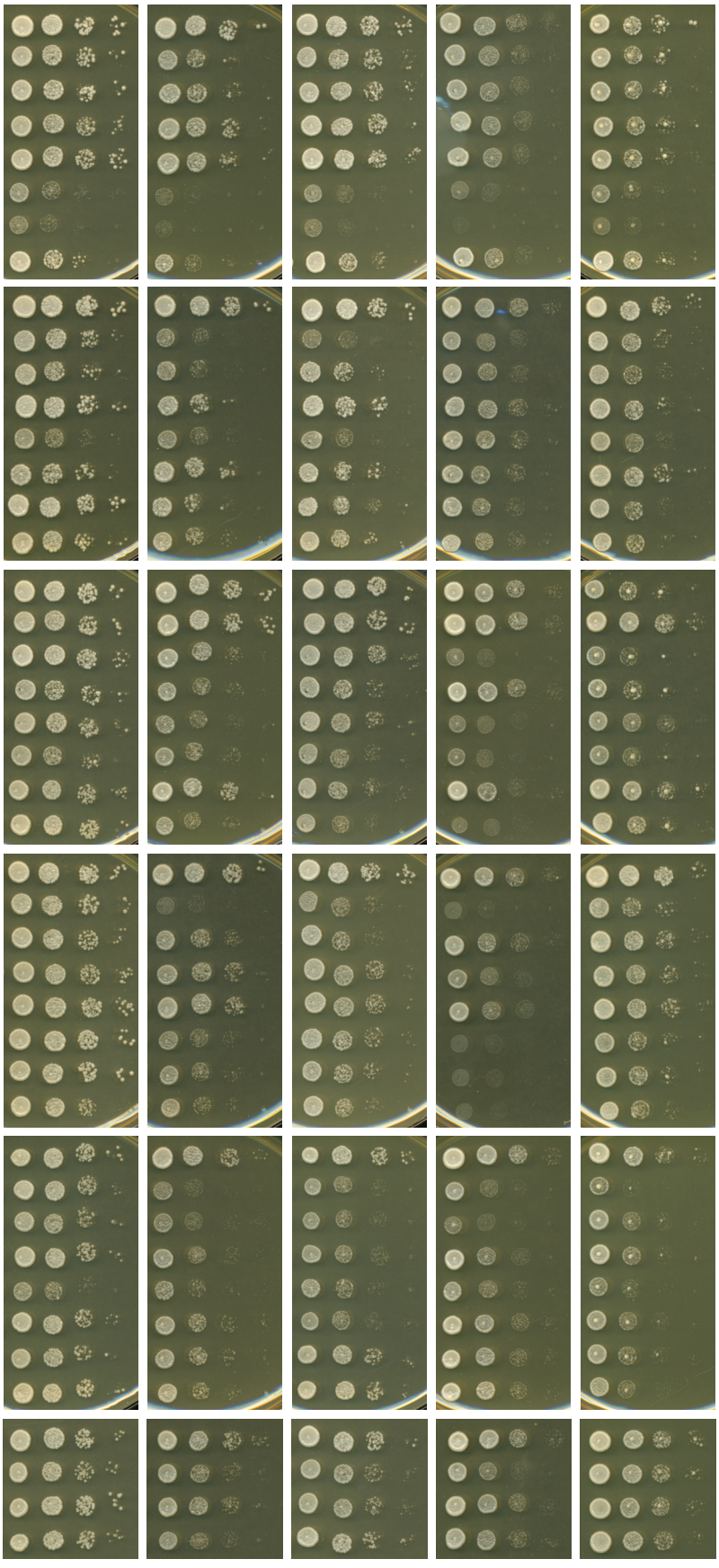
YPD
15 µg/ml CPT
0.3 µg/ml Phleo
.01% MMS
100 J/m² UV
WT (1N)
A2
A3
A4
A5
A6
A7
A8
WT (1N)
1N+II, XII
1N+I, II, XII
1N+I, II, IX, XI
1N+II, IX, XI
1N+II, III, V, VII, IX, XI, XII, XIV, XV, XVI
1N+II, IV, V , VII, VIII, X, XI, XII, XIII, XV, XVI
1N+II, III, III, IX, IX
WT (1N)
A9
A10
A11
A12
A13
A14
A15
WT (1N)
1N+II, XIII, XVI
1N+III, XI, XII, XV
1N+III, XVI
1N+I, II, III, IV, VII, VIII, IX, X, XI, XII, XIV, XV, XVI
1N+I, II, VIII, XI, XIII
1N+IX, XVI
1N+II, III, VII, IX, XI, XII
WT (1N)
WT (2N)
A16
A17
A18
A19
A20
A21
WT (1N)
WT (2N)
1N+XIII
1N+II, III, V
2N+V, VII, IX, X, XI, XVI
2N+I, II, VII, IX, X, XII, XIII, XIV
2N+VII, IX, XIII, XIV, XV
2N+II, IV, VII, XIII, XIV, XV
WT (2N)
A22
A23
A24
A25
A26
A27
A28
WT (2N)
2N+II, IV, VII, VIII, X, XI, XIV, XV, XVI
2N+I, II, IX, XI, XII, XIII, XIV, XV
2N+II, VII, IX, XIV
2N+II, VII, XIV
2N+II, X, XI, XIII, XIV
2N+II, X, XI, XIII, XIV
2N+II, VI, VII, VIII, IX, X, XI, XIII
WT (2N)
A29
A30
A31
A32
A33
A34
A35
WT (2N)
2N+II, VI, VII, IX, X, XIII, XVI
2N+I, II, VI, VII, VIII, IX, XI, XIII, XIV, XVI
2N+II, VI, VII, XIII, XIV, XV, XVI
2N+I, IV, VIII, IX, X, XI
2N+II, VI, VII, XIII, XIV, XV, XVI
2N+I, IV, VIII, IX, X, XI
2N+I, V, VII, IX, XI, XII
WT (2N)
A36
A37
A38
WT (2N)
2N+VII, VIII, X, XI, XIII, XV, XVI
2N+II, VII, XIV, XV, XVI
2N+II, IV, VIII, IX, XI, XV

Figure S4. Aneuploid strains derived from triploid meioses are sensitive to genotoxic damage. 10-fold serial dilutions of the indicated strains were spotted on either YPD medium or medium supplemented or treated with the indicated genotoxic agent. The karyotype of these strains is indicated to the right of the figure. CPT; camptothecin. Phleo; phleomycin. MMS, methyl methanesulfonate. The construction and nomenclature of these strains are described in *(26)*. Note that in many strains the reported karyotype is present in only a subset of the cells, and some strains have euploid or near-euploid subpopulations (fig S13 and S14).

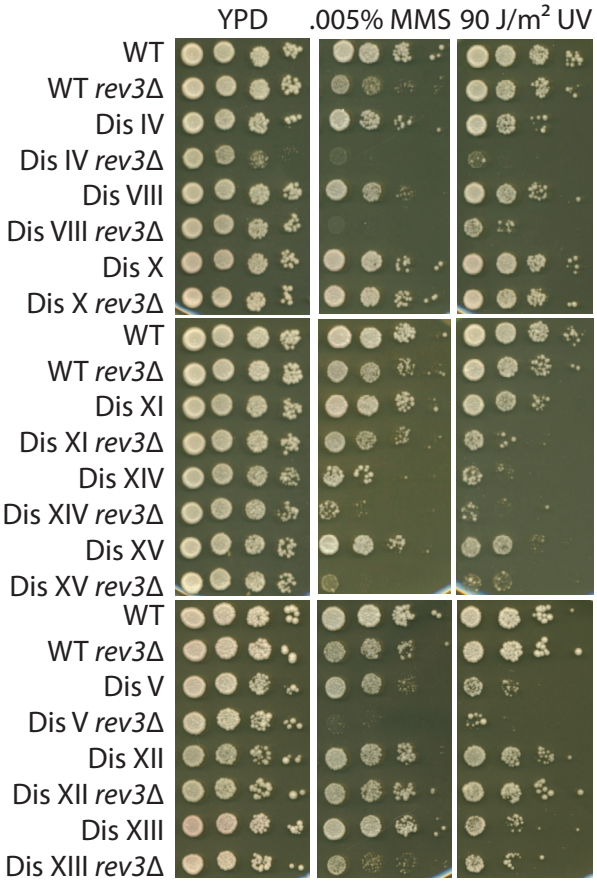

Figure S5. Several disomes require Polζ to survive DNA damage. 10-fold serial dilutions of the indicated *REV3* and *rev3*Δ strains were spotted on either YPD medium or medium supplemented or treated with the indicated genotoxic agent. Most disomes that lack *REV3* are hypersensitive to low doses of DNA damaging agents. MMS, methyl methanesulfonate. Strains (from the top): A11311, A25391, A12687, A25392, A13628, A25393, A12689, A25394, A13771, A25395, A13979, A25396, A12697, A25397, A14479, A26629, A12693, A26630, A21987, and A26631.

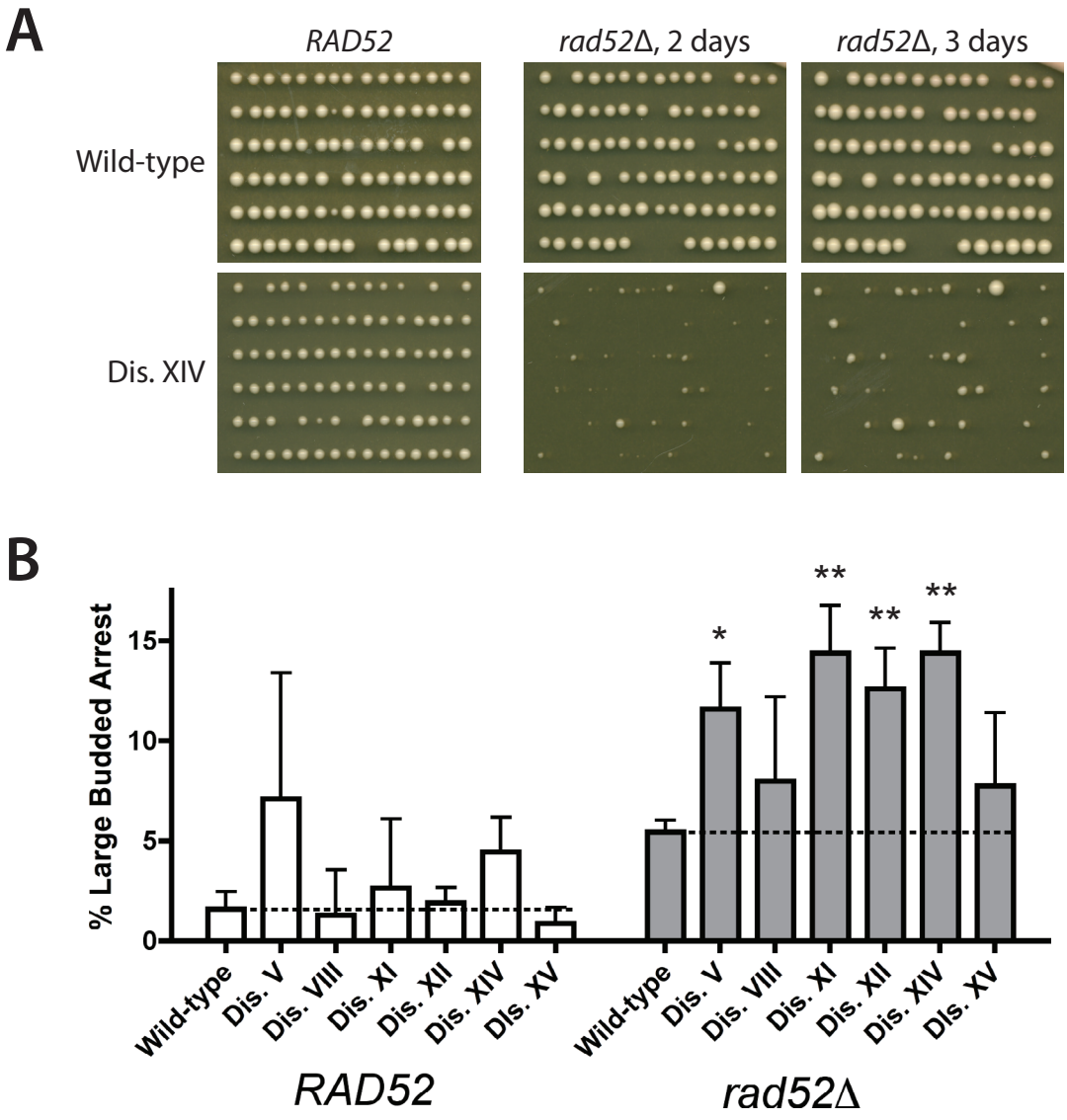

Figure S6. Some disomes acquire double-strand breaks more frequently during DNA replication. Small budded cells were isolated by micromanipulation on YPD plates and incubated for 5 hours at 30ºC. Subsequently, the cells were examined under a microscope, and the number of cells that were arrested as large buds and the number of cells that had successfully divided were scored. Cells which had not progressed beyond the small-budded stage were excluded from analysis. **(A)** Representative plates of euploid *RAD52*, euploid *rad52*Δ, disome XIV *RAD52*, and disome XIV *rad52*Δ are displayed. Plates containing *RAD52* cells were scanned after 2 days of growth, while plates containing *rad52*Δ cells were scanned after 2 or 3 days of growth. **(B)** The percentage of cells arrested as large buds is displayed. The mean and standard deviation of 3 independent experiments are shown. Strains (from the left): A15546, A27223, A15533, A15537, A15538, A15540, A15542, A26504, A28064, A19616, A27091, A19618, A19619, and A19620.

A

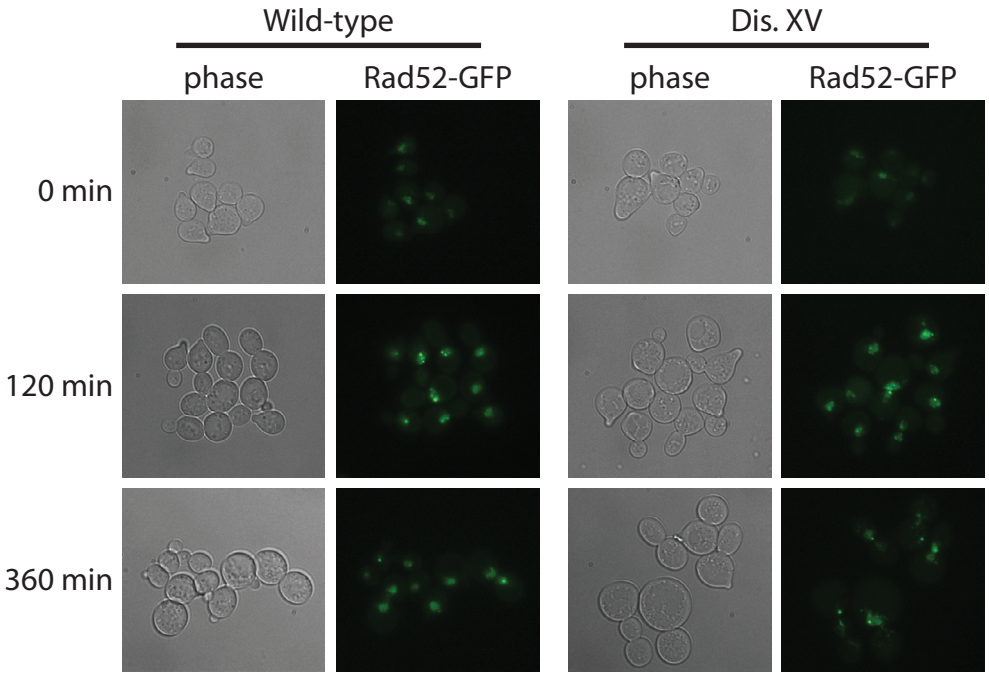
Wild-type
Dis. XV
phase
Rad52-GFP
phase
Rad52-GFP
0 min
120 min
360 min

B

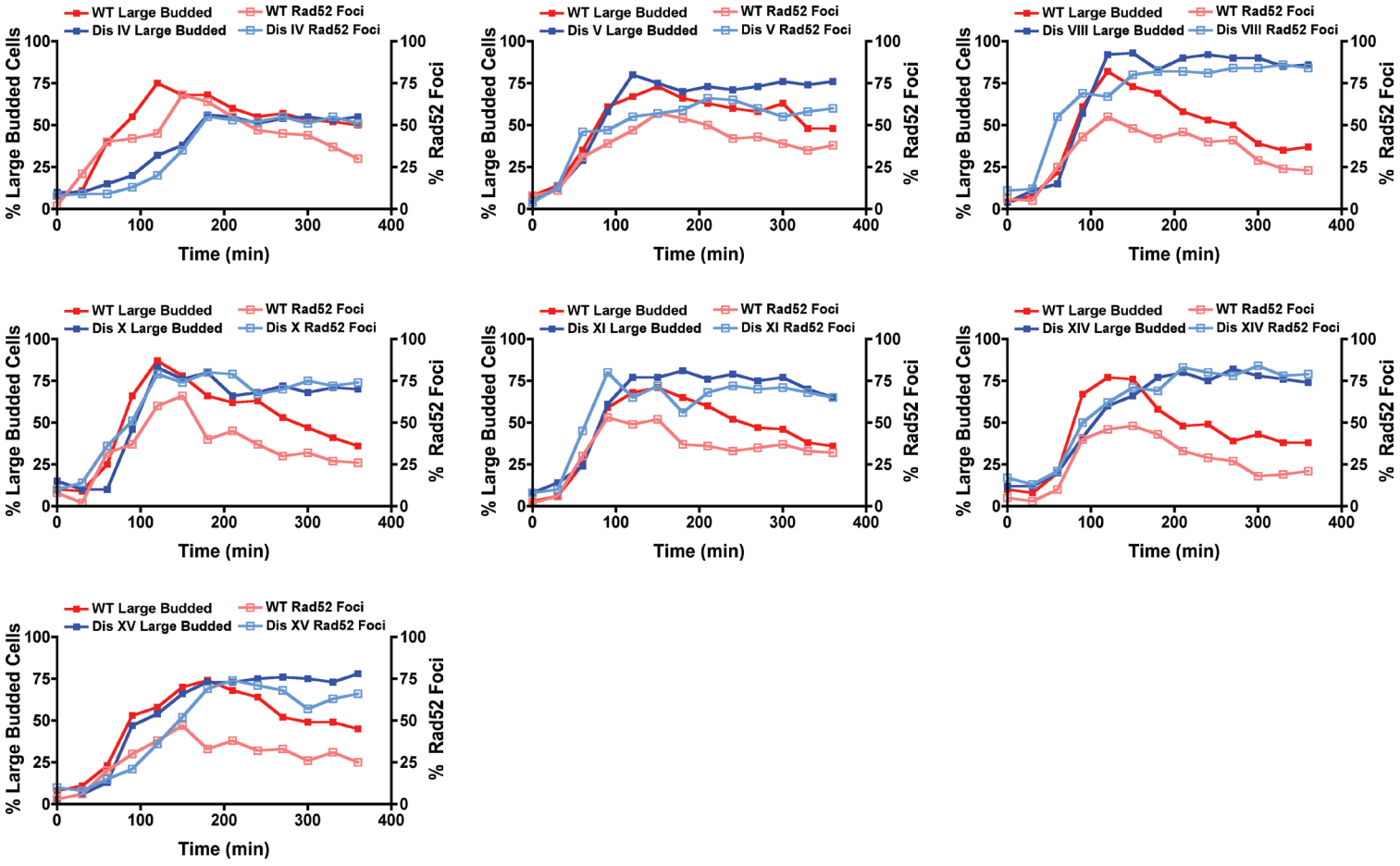
WT Large Budded
WT Rad52 Foci
Dis IV Large Budded
Dis IV Rad52 Foci
Dis V Large Budded
Dis V Rad52 Foci
Dis VIII Large Budded
Dis VIII Rad52 Foci
Dis X Large Budded
Dis X Rad52 Foci
Dis XI Large Budded
Dis XI Rad52 Foci
Dis XIV Large Budded
Dis XIV Rad52 Foci
Dis XV Large Budded
Dis XV Rad52 Foci
% Large Budded Cells
% Rad52 Foci
Time (min)
0
25
50
75
100
100
200
300
400

Figure S7. Disomes are unable to repair phleomycin-induced lesions. Strains were arrested in G1 with pheromone, then released into medium containing 0.15μg/ml phleomycin. After 135 minutes, the cells were washed and resuspended in medium lacking phleomycin. Cells were removed every 30 minutes to determine the percentage of large-budded cells (closed symbols) and the percentage of cells with Rad52-GFP foci (open symbols). **(A)** Representative images of wild-type and Dis. XV cells after G1 arrest (top), after growth in the presence of phleomycin (middle), and after 4 hours of recovery in phleomycin-free medium (bottom). **(B)** Phleomycin arrest/release results for Dis. IV (A26532), V (A26533), VIII (A25342), X (A25343), XI (A25421), XIV (A25344), and XV (A25355). Note that Dis. IV cells display a severe G1 delay *(1)*, and many cells failed to bud during the course of the experiment. The Dis. IV cells that did bud were arrested as large-budded cells by phleomycin and almost all remained arrested for the duration of the time course.

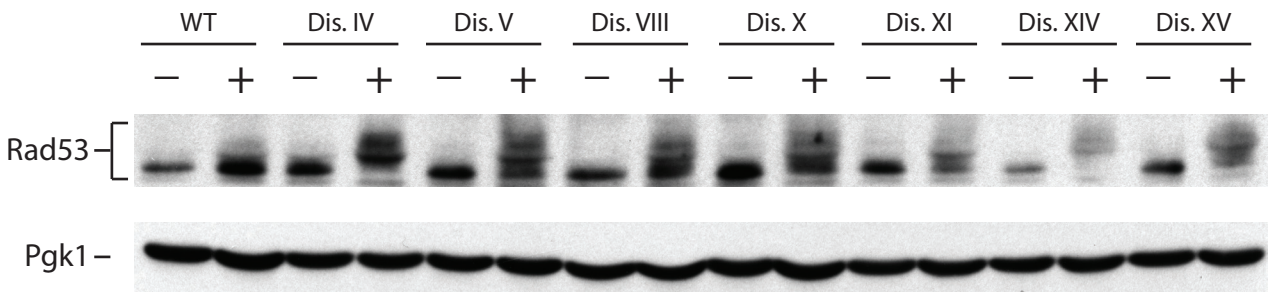

Figure S8. Disomic yeast strains phosphorylate Rad53 in response to phleomycin treatment. Rad53 mobility on SDS-PAGE was examined in untreated exponentially growing cells and in exponentially growing cells that were treated with 0.3µg/ml phleomycin for 90 minutes. The slower migrating forms of Rad53 represent phosphorylated Rad53. Pgk1 was used as a loading control. Strains (from the left): A11311, A12687, A14479, A13628, A21986, A13771, A13979, and A12697.

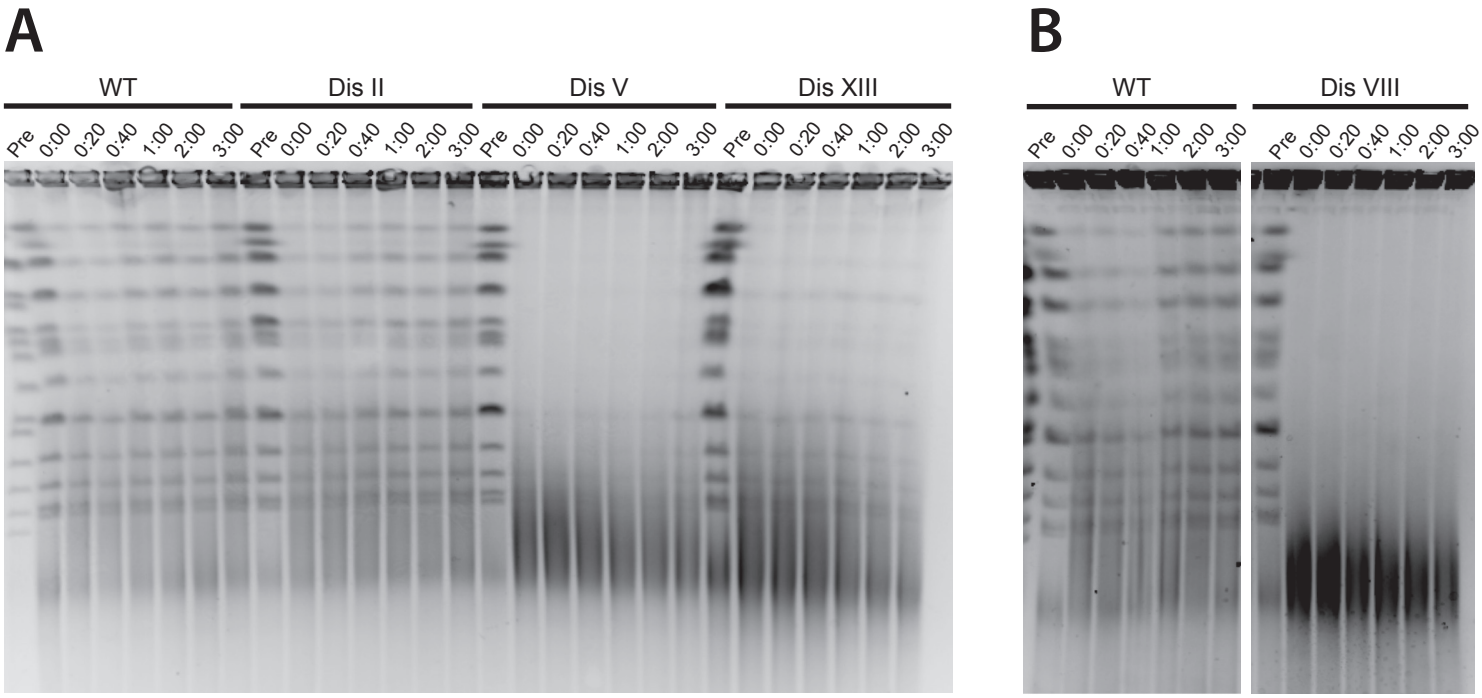

Figure S9. Disomic yeast strains display delayed chromosomal recovery following phleomycin treatment. Wild-type and disomic strains were treated with 25µg/ml phleomycin for 2 hours, then washed with 5 volumes of medium and released into YPD medium containing 15µg/ml nocodazole. Nocodazole was used to keep the number of cells in culture constant during recovery. Before treatment ("pre"), immediately following phleomycin wash-out ("0:00"), and at the indicated times after phleomycin wash-out cells were fixed with sodium azide and chromosomes were examined by pulse-field gel electrophoresis. Intact chromosomes are visible as discrete bands, while chromosome fragments run as a smear at the bottom of the gel or do not enter the gel. Strains (from the left): **(A)** A11311, A12685, A14479, A21987. **(B)** A11311 and A13628.

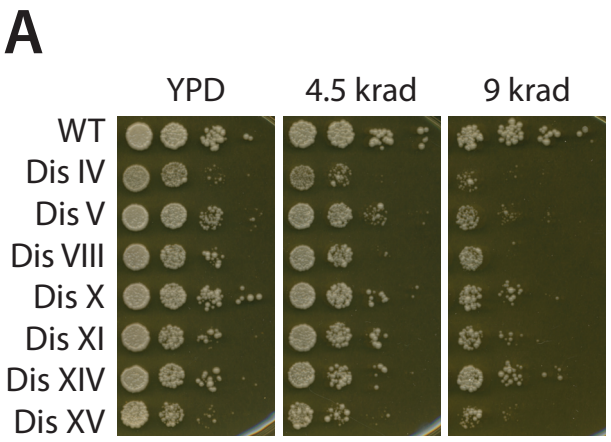
A
YPD
4.5 krad
9 krad
WT
Dis IV
Dis V
Dis VIII
Dis X
Dis XI
Dis XIV
Dis XV

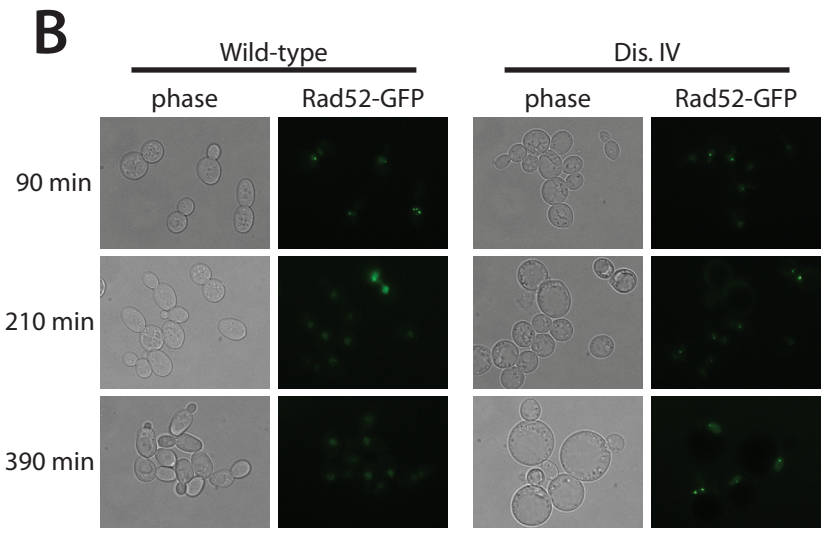
B
Wild-type
Dis. IV
phase
Rad52-GFP
phase
Rad52-GFP
90 min
210 min
390 min

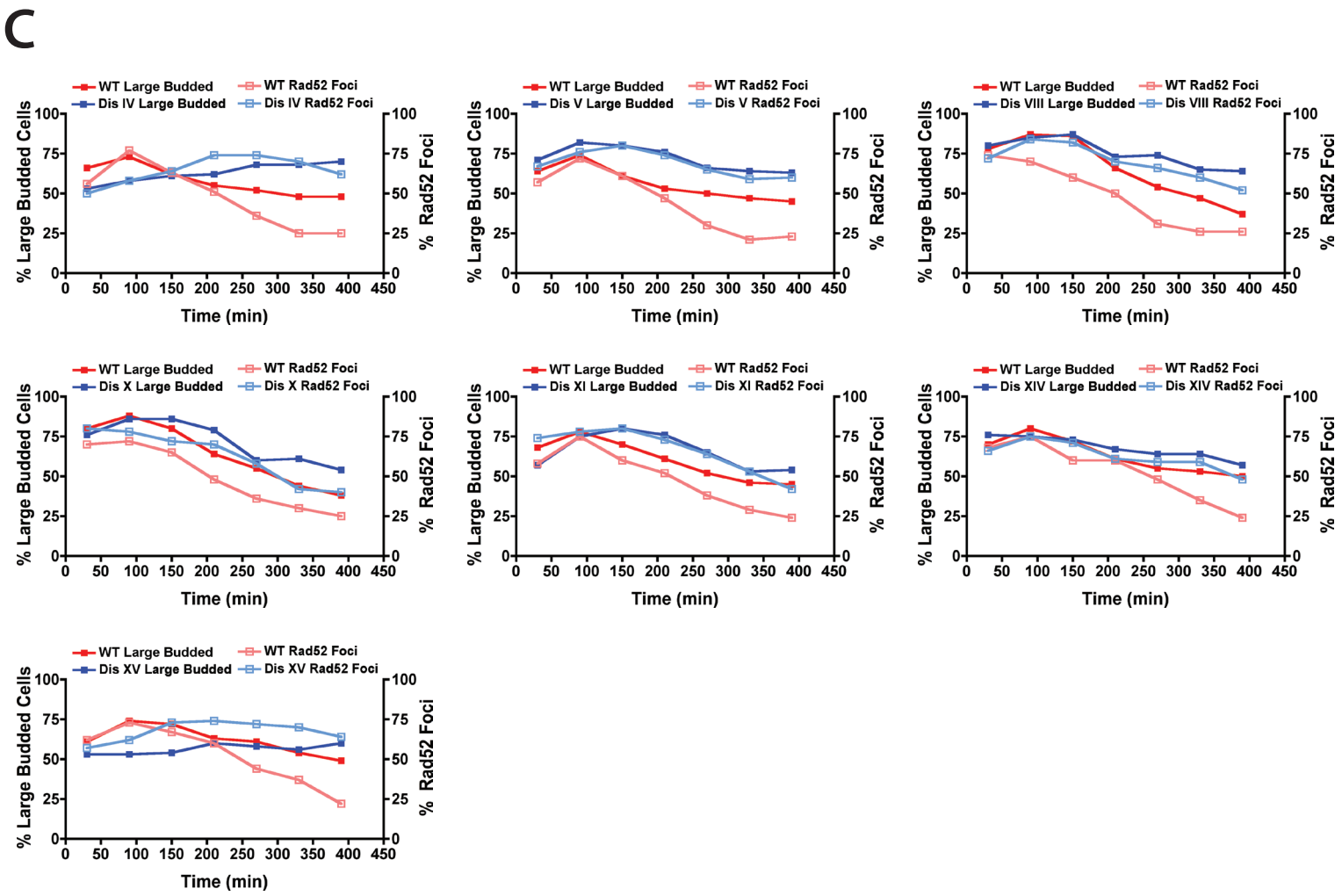
C
WT Large Budded
WT Rad52 Foci
Dis IV Large Budded
Dis IV Rad52 Foci
Dis V Large Budded
Dis V Rad52 Foci
Dis VIII Large Budded
Dis VIII Rad52 Foci
Dis X Large Budded
Dis X Rad52 Foci
Dis XI Large Budded
Dis XI Rad52 Foci
Dis XIV Large Budded
Dis XIV Rad52 Foci
Dis XV Large Budded
Dis XV Rad52 Foci
% Large Budded Cells
% Rad52 Foci
Time (min)

Figure S10. Disomic yeast strains are impaired in the repair of damage caused by ionizing radiation. **(A)** 10-fold serial dilutions of the indicated strains were spotted on YPD medium and then treated with the indicated dose of radiation. Strains (from the top): A24352, A26532, A26533, A25342, 25343, A25421, A25344, and A25355. **(B)** Exponentially-growing cultures were treated with 4.5krads of radiation and then allowed to recover. Cells were removed every 60 minutes to determine the percentage of large-budded cells (closed symbols) and the percentage of cells with Rad52-GFP foci (open symbols). Representative images of wild-type and Dis. IV cells are shown 90 minutes after treatment with radiation (top), after 210 minutes of recovery (middle), and after 390 minutes of recovery (bottom). **(B)** Radiation recovery results for Dis. IV (A26532), V (A26533), VIII (A25342), X (25343), XI (A25421), XIV (A25344), and XV (A25355).

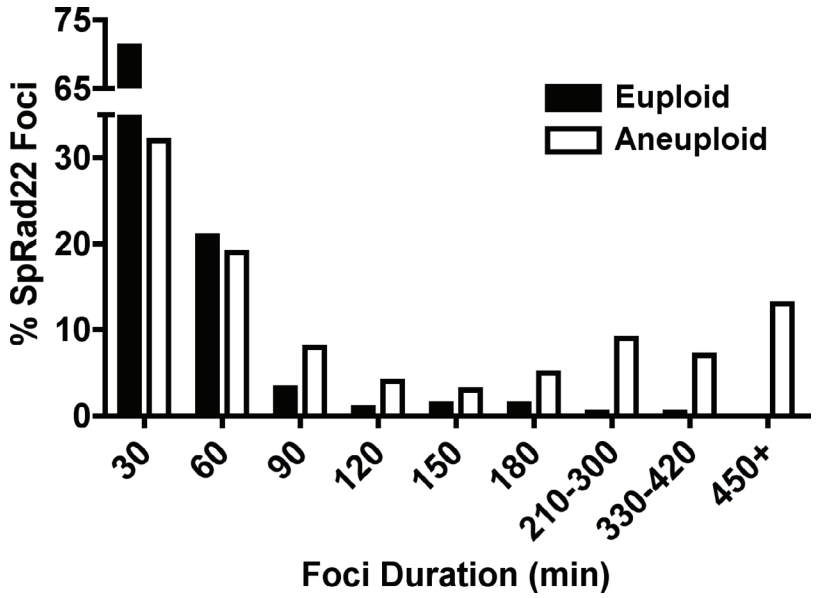

Microcolony Type	Mean Focus Duration in Minutes (+/- SD)	Number of Foci	% Cells which Divide without Foci Formation	Number of Cells
Euploid	45.6 (+/- 39.6)	215	53.8%	470
Aneuploid	219.8 (+/- 367.0)***	100	47.5%	141

*** p<.0005 (Wilcoxon rank-sum test)

Figure S11. Persistence of SpRad22-GFP foci duration in aneuploid strains of *S. pombe*. The time that SpRad22-GFP foci persisted in cells was measured in euploid and aneuploid strains generated from a triploid meiosis. Aneuploid cells were identified by their delayed germination and aberrant colony morphology. Cells were imaged every 30 minutes.

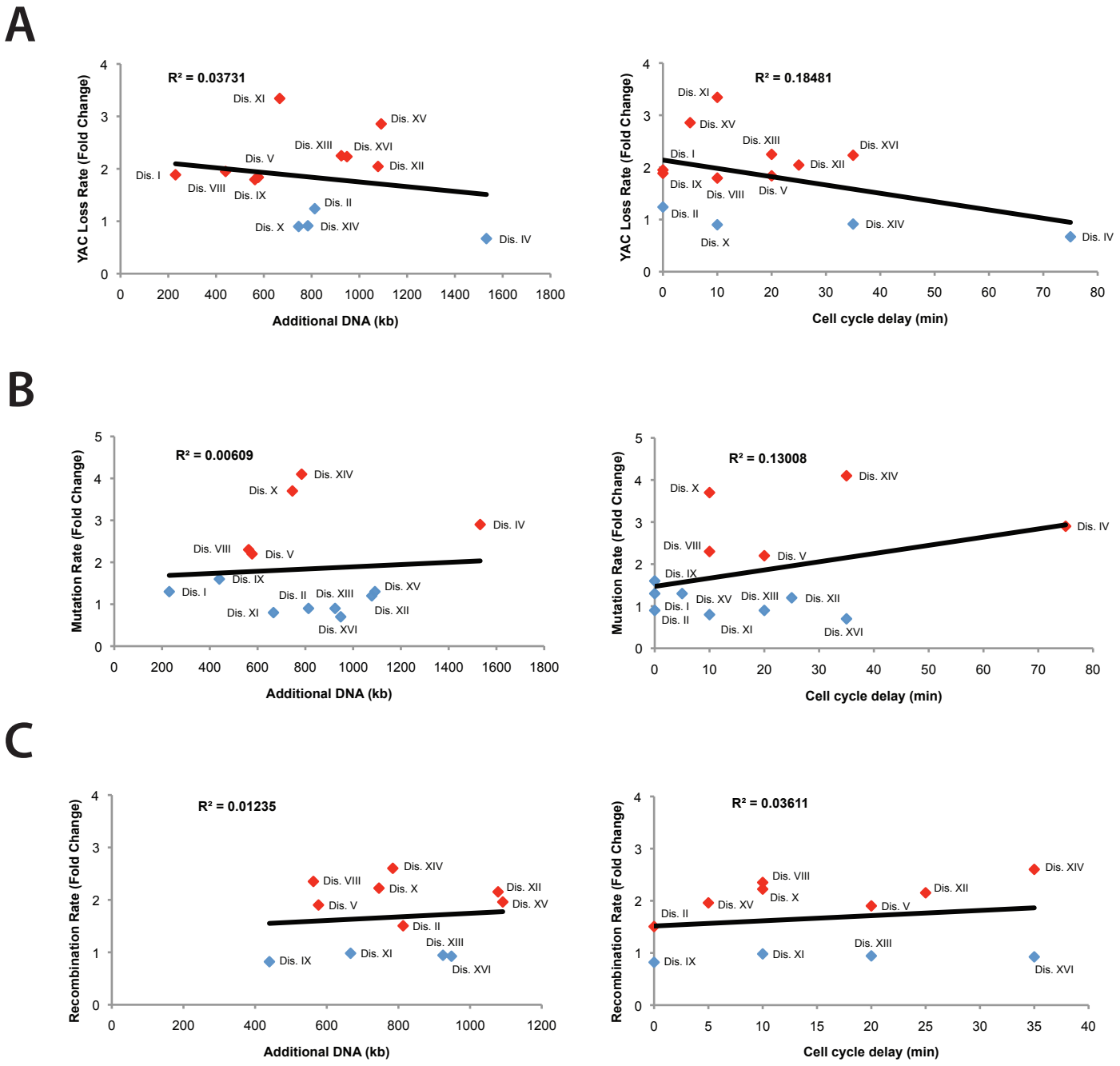

Fig. S12. Genomic instability is not correlated with the size of the extra chromosome or the cell cycle delay in disomic strains. Linear regression analysis (black line) reveals that the fold increase in **(A)** chromosome missegregation, **(B)** forward mutation, and **(C)** mitotic recombination are independent of the size of the extra chromosome and the cell cycle delay in the disomic strains. Cell cycle delay data are from *(1)*.

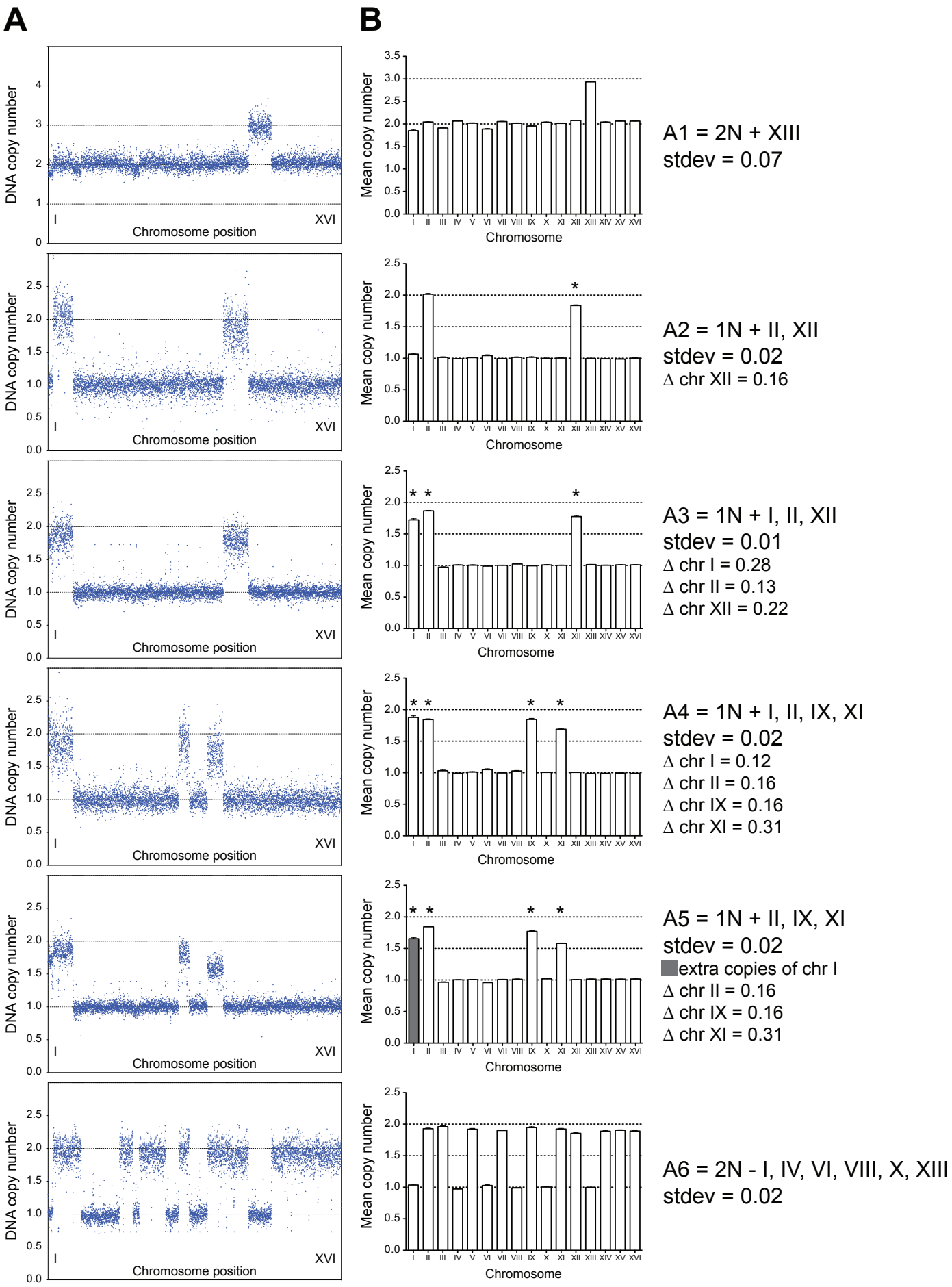
A
B
DNA copy number
Chromosome position
I
XVI
Mean copy number
Chromosome
I II III IV V VI VII VIII IX X XI XII XIII XIV XV XVI
A1 = 2N + XIII
stdev = 0.07
A2 = 1N + II, XII
stdev = 0.02
Δ chr XII = 0.16
A3 = 1N + I, II, XII
stdev = 0.01
Δ chr I = 0.28
Δ chr II = 0.13
Δ chr XII = 0.22
A4 = 1N + I, II, IX, XI
stdev = 0.02
Δ chr I = 0.12
Δ chr II = 0.16
Δ chr IX = 0.16
Δ chr XI = 0.31
A5 = 1N + II, IX, XI
stdev = 0.02
extra copies of chr I
Δ chr II = 0.16
Δ chr IX = 0.16
Δ chr XI = 0.31
A6 = 2N - I, IV, VI, VIII, X, XIII
stdev = 0.02

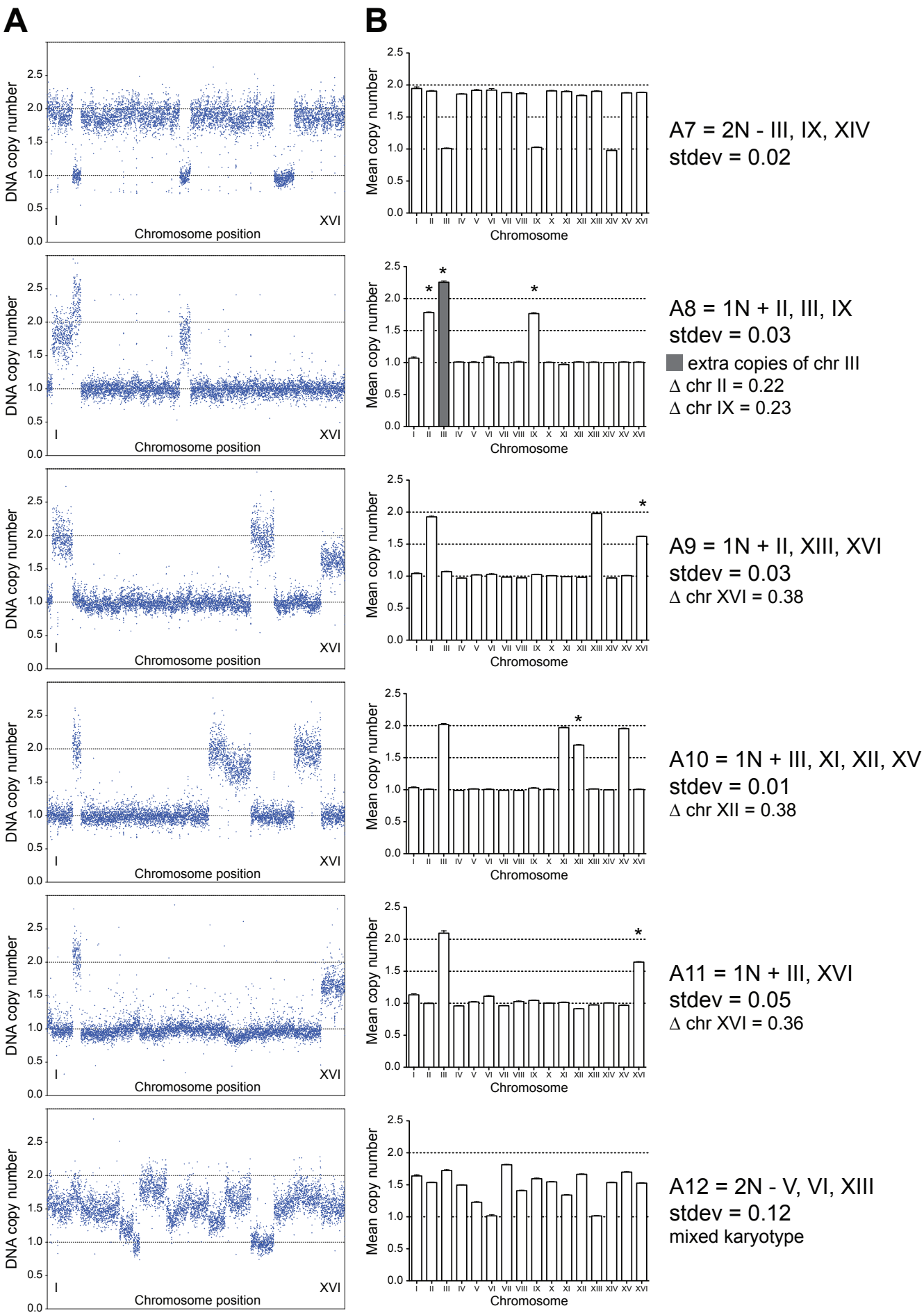
A
B
DNA copy number
Chromosome position
I
XVI
Mean copy number
Chromosome
I II III IV V VI VII VIII IX X XI XII XIII XIV XV XVI
A7 = 2N - III, IX, XIV
stdev = 0.02
A8 = 1N + II, III, IX
stdev = 0.03
extra copies of chr III
Δ chr II = 0.22
Δ chr IX = 0.23
A9 = 1N + II, XIII, XVI
stdev = 0.03
Δ chr XVI = 0.38
A10 = 1N + III, XI, XII, XV
stdev = 0.01
Δ chr XII = 0.38
A11 = 1N + III, XVI
stdev = 0.05
Δ chr XVI = 0.36
A12 = 2N - V, VI, XIII
stdev = 0.12
mixed karyotype

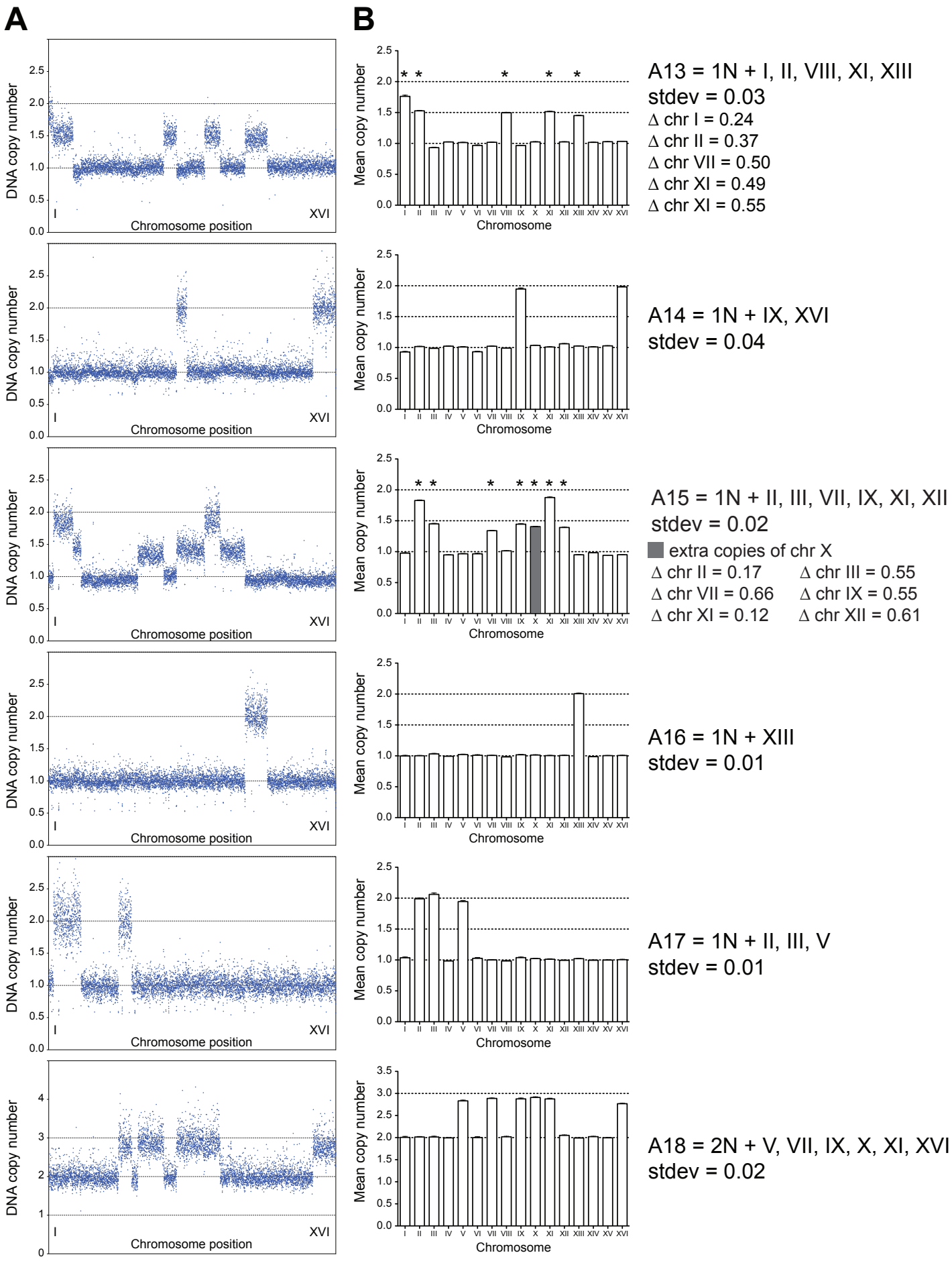
A
B
DNA copy number
Chromosome position
I
XVI
Mean copy number
Chromosome
I II III IV V VI VII VIII IX X XI XII XIII XIV XV XVI
A13 = 1N + I, II, VIII, XI, XIII
stdev = 0.03
Δ chr I = 0.24
Δ chr II = 0.37
Δ chr VII = 0.50
Δ chr XI = 0.49
Δ chr XI = 0.55
A14 = 1N + IX, XVI
stdev = 0.04
A15 = 1N + II, III, VII, IX, XI, XII
stdev = 0.02
extra copies of chr X
Δ chr II = 0.17
Δ chr III = 0.55
Δ chr VII = 0.66
Δ chr IX = 0.55
Δ chr XI = 0.12
Δ chr XII = 0.61
A16 = 1N + XIII
stdev = 0.01
A17 = 1N + II, III, V
stdev = 0.01
A18 = 2N + V, VII, IX, X, XI, XVI
stdev = 0.02

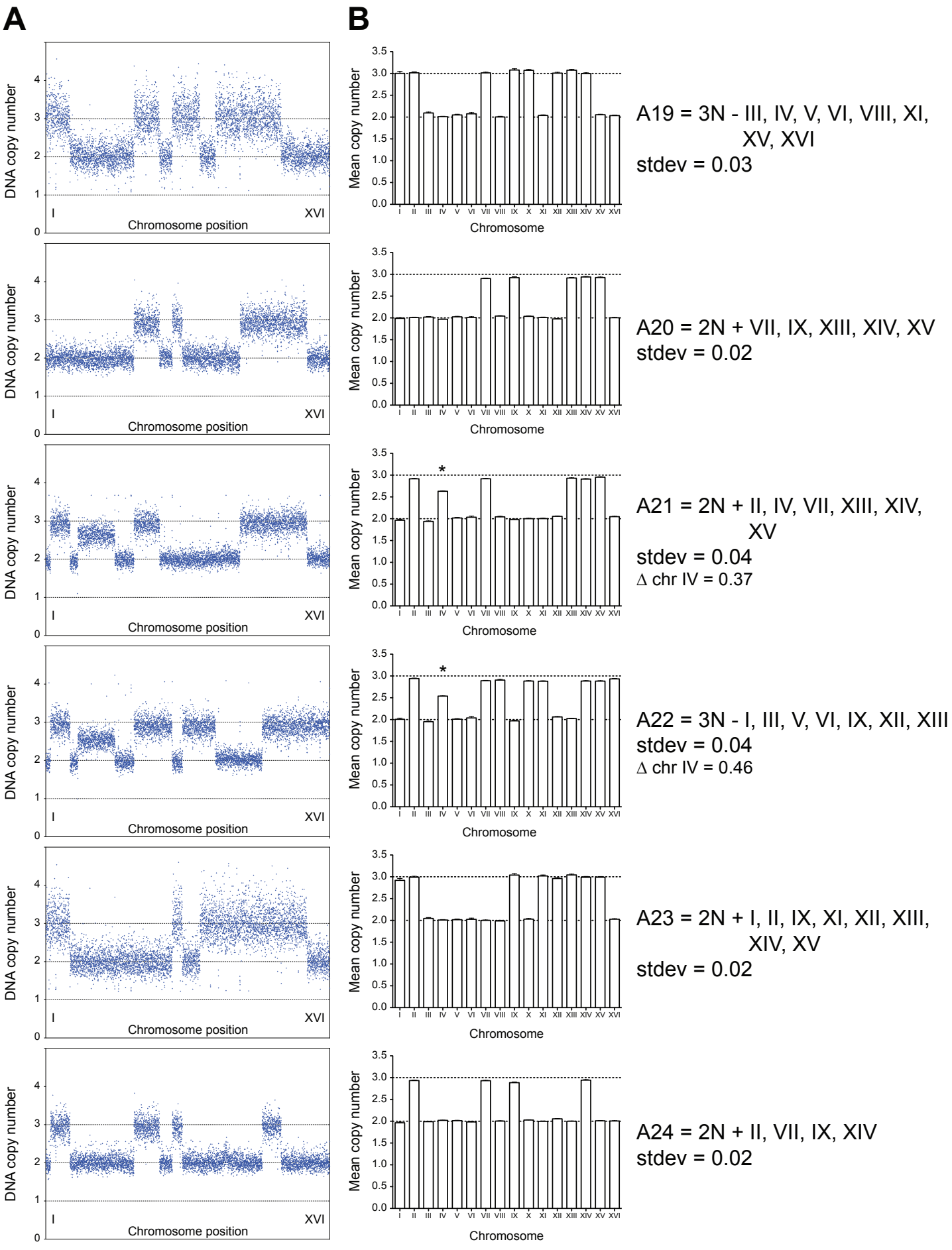
A
B
DNA copy number
Chromosome position
I
XVI
Mean copy number
Chromosome
I II III IV V VI VII VIII IX X XI XII XIII XIV XV XVI
*
A19 = 3N - III, IV, V, VI, VIII, XI, XV, XVI
stdev = 0.03
A20 = 2N + VII, IX, XIII, XIV, XV
stdev = 0.02
A21 = 2N + II, IV, VII, XIII, XIV, XV
stdev = 0.04
Δ chr IV = 0.37
A22 = 3N - I, III, V, VI, IX, XII, XIII
stdev = 0.04
Δ chr IV = 0.46
A23 = 2N + I, II, IX, XI, XII, XIII, XIV, XV
stdev = 0.02
A24 = 2N + II, VII, IX, XIV
stdev = 0.02

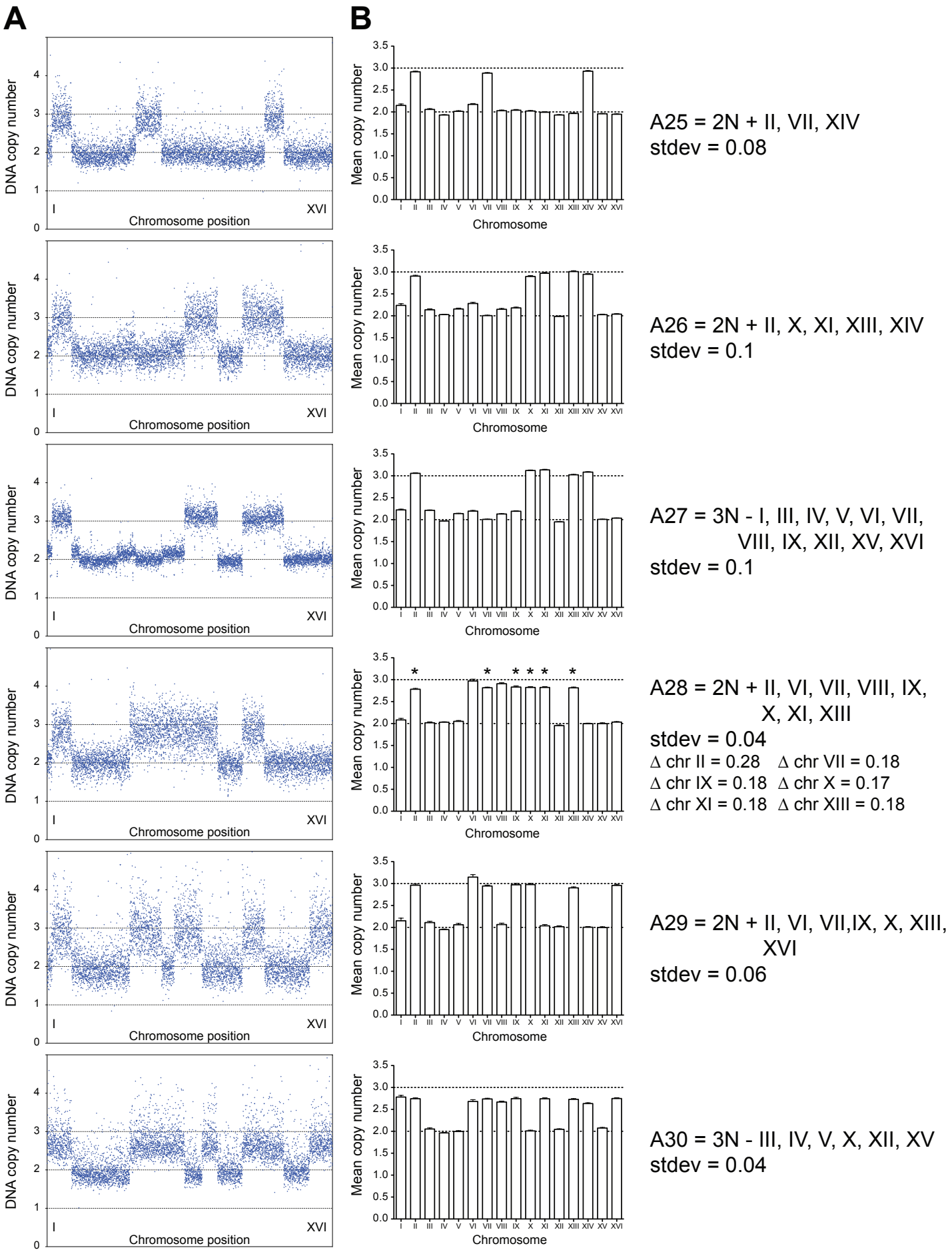
A
B
DNA copy number
Chromosome position
I
XVI
Mean copy number
Chromosome
I II III IV V VI VII VIII IX X XI XII XIII XIV XV XVI
A25 = 2N + II, VII, XIV
stdev = 0.08
A26 = 2N + II, X, XI, XIII, XIV
stdev = 0.1
A27 = 3N - I, III, IV, V, VI, VII, VIII, IX, XII, XV, XVI
stdev = 0.1
A28 = 2N + II, VI, VII, VIII, IX, X, XI, XIII
stdev = 0.04
Δ chr II = 0.28 Δ chr VII = 0.18
Δ chr IX = 0.18 Δ chr X = 0.17
Δ chr XI = 0.18 Δ chr XIII = 0.18
A29 = 2N + II, VI, VII,IX, X, XIII, XVI
stdev = 0.06
A30 = 3N - III, IV, V, X, XII, XV
stdev = 0.04

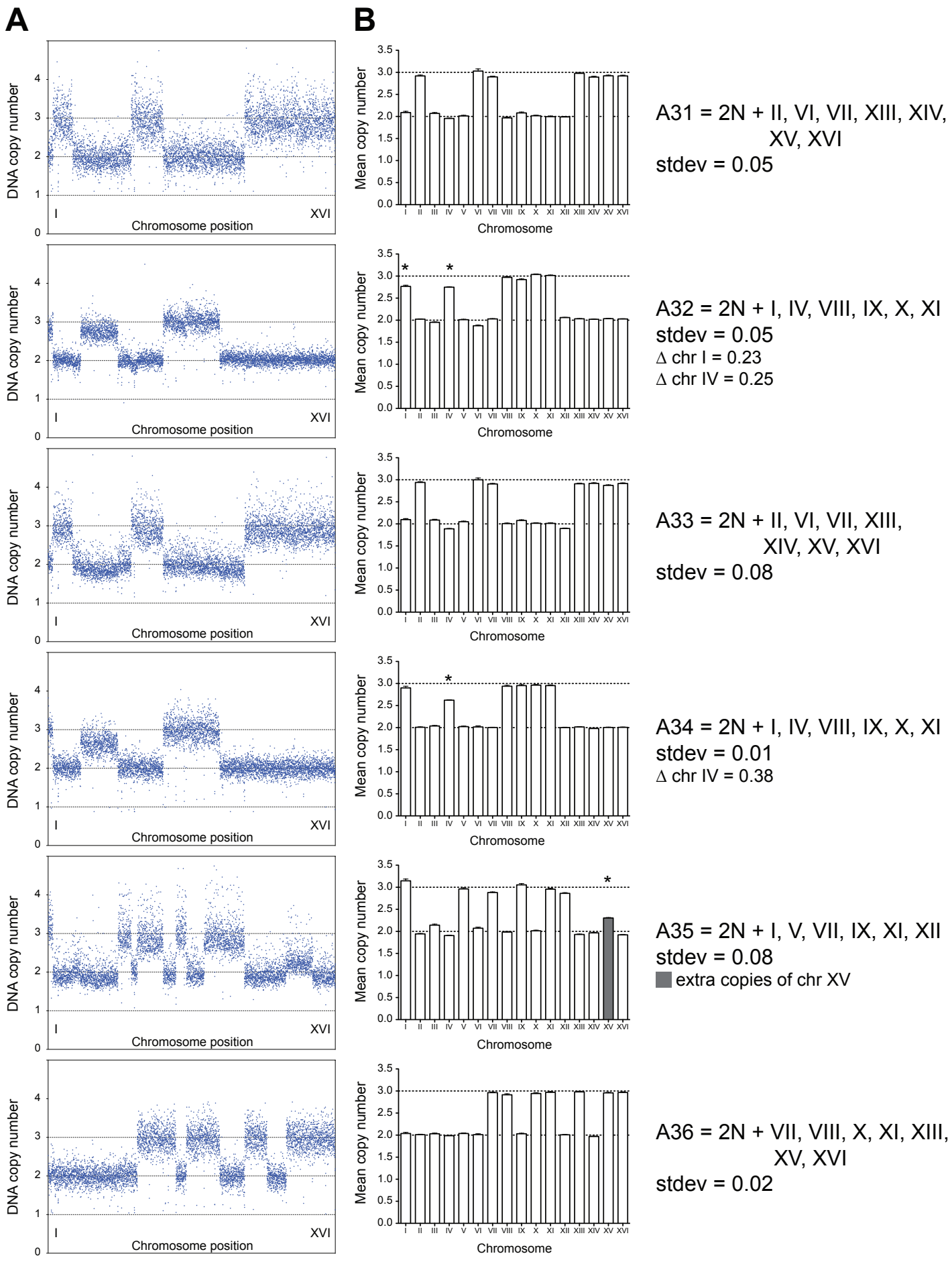
A
B
DNA copy number
Chromosome position
I
XVI
Mean copy number
Chromosome
I II III IV V VI VII VIII IX X XI XII XIII XIV XV XVI
A31 = 2N + II, VI, VII, XIII, XIV, XV, XVI
stdev = 0.05
A32 = 2N + I, IV, VIII, IX, X, XI
stdev = 0.05
Δ chr I = 0.23
Δ chr IV = 0.25
A33 = 2N + II, VI, VII, XIII, XIV, XV, XVI
stdev = 0.08
A34 = 2N + I, IV, VIII, IX, X, XI
stdev = 0.01
Δ chr IV = 0.38
A35 = 2N + I, V, VII, IX, XI, XII
stdev = 0.08
extra copies of chr XV
A36 = 2N + VII, VIII, X, XI, XIII, XV, XVI
stdev = 0.02

A

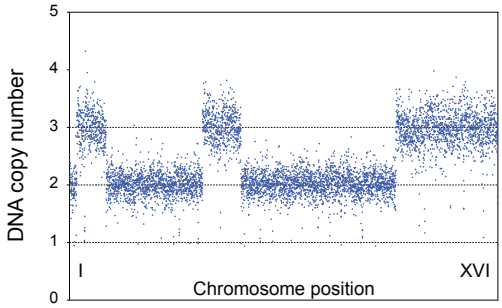

B

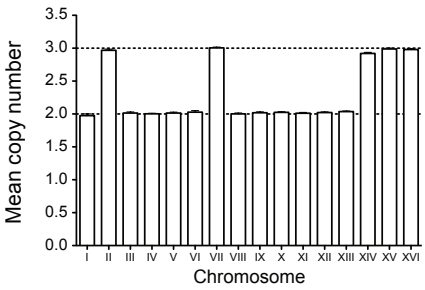

A37 = 2N + II, VII, XIV, XV, XVI
stdev = 0.02

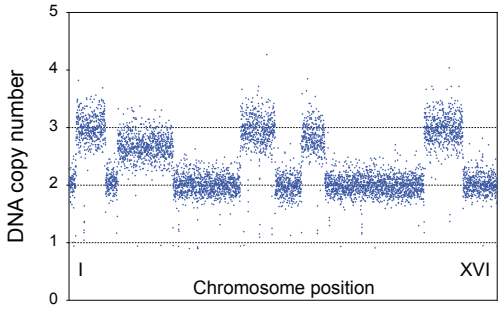

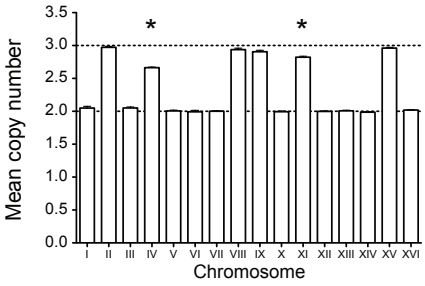

A38 = 2N + II, IV, VIII, IX, XI, XV
stdev = 0.02
Δ chr IV = 0.34
Δ chr XI = 0.18

Figure S13. DNA content analysis of aneuploid strains derived from triploid meiosis. Pavelka et al. *(26)* recently reported the analysis of aneuploid yeast strains obtained as meiotic products from triploid and pentaploid strains. 87.5% of these strains were discarded due to chromosomal instability, but 38 yeast strains were described as karyotypically stable. To determine whether these aneuploid strains displayed homogenous karyotypes, we determined their DNA content via comparative genomic hybridization (CGH) analysis as described in the Supplemental Methods. **(A)** CGH analysis of the 38 strains characterized in *(26)*. Each box represents the genome of an aneuploid yeast strain. Data points are ordered according to their chromosomal coordinates, starting with the gene most distally located on the left arm of chromosome I. DNA copy number was calculated from the log2 ratios of the DNA content of aneuploid strains relative to an isogenic euploid strain. 17 of the 38 aneuploid strains did not display a homogeneous karyotype. The copy number of certain chromosomes was not an integer multiple of the haploid value, indicating that different cells in the population carry a different copy number of that particular chromosome(s). **(B)** Average copy numbers calculated per chromosome are shown. Error bars represent the standard error of the mean per chromosome. Standard deviations (stdev) of the mean values of the euploid chromosomes are shown. The difference (Δ) between the expected value and the measured copy number is shown. Chromosomes where this difference was at least 4 times greater than the standard deviation of the euploid chromosomes are marked with an asterisk. In 4 strains, a subset of cells had gained extra copies of a chromosome; aneuploid chromosomes that were not reported in *(26)* are highlighted in grey. Note that the under-representation of the marked chromosomes cannot be explained by a dramatic decrease in signal of a few data points, because the decreased values are consistent across the chromosome. It is also not due to variability in the experimental procedure. The standard deviations of the means of the euploid chromosomes were consistently small and we only considered chromosomes as being under- or over-represented when the deviation from the expected value was at least 4-fold greater than the standard deviation of the means of the euploid chromosomes. In most cases the difference was in fact greater than 8-fold. The observation that these strains display heterogenous karyotypes, including both chromosome gains and losses, strongly suggests that they are karyotypically unstable.

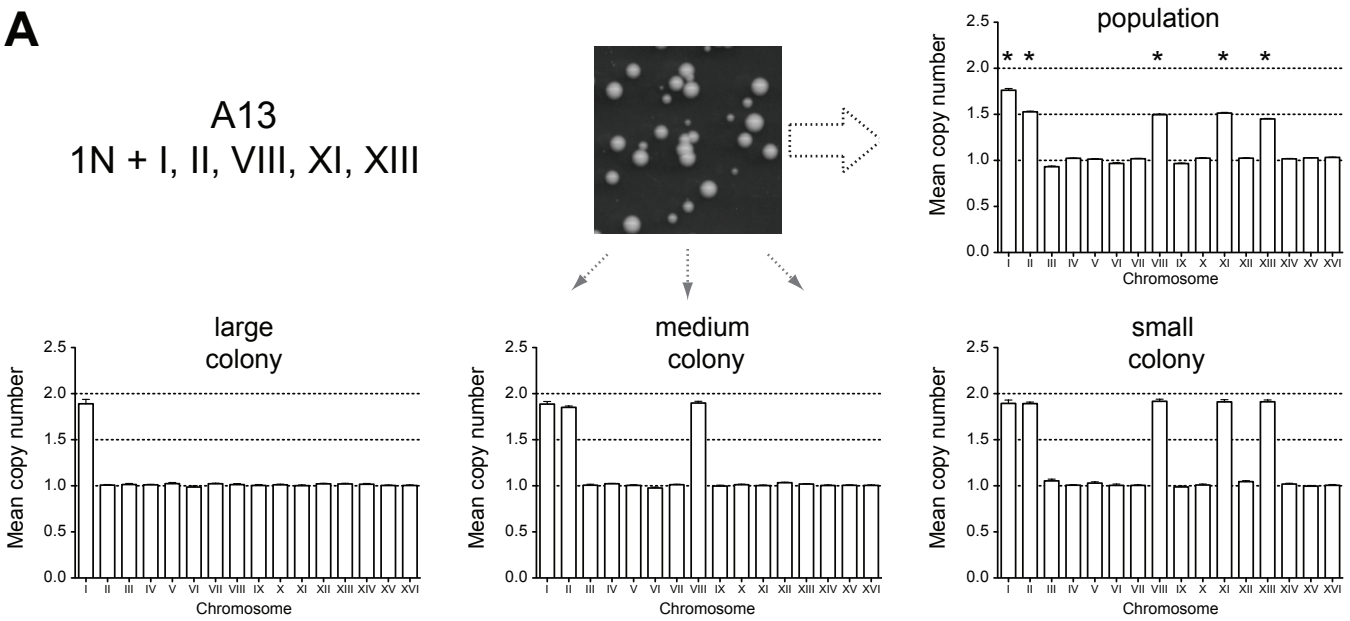
A
A13
1N + I, II, VIII, XI, XIII
population
large colony
medium colony
small colony
Mean copy number
Chromosome
I II III IV V VI VII VIII IX X XI XII XIII XIV XV XVI

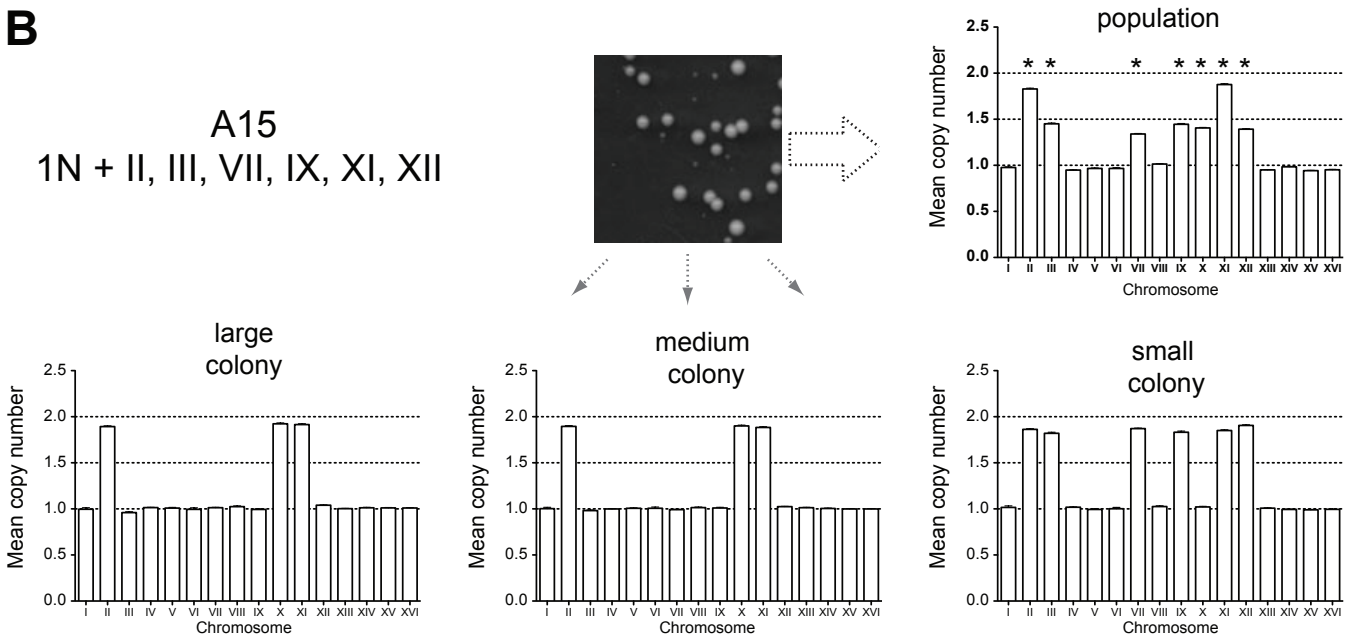
B
A15
1N + II, III, VII, IX, XI, XII
population
large colony
medium colony
small colony
Mean copy number
Chromosome
I II III IV V VI VII VIII IX X XI XII XIII XIV XV XVI

Figure S14. Strains A13 and A15 are heterogeneous. **(A)** We noted that single colonies derived from the strains described in *(26)* frequently displayed significant variation in colony size during routine growth on rich medium. Representative images of single colonies from strains A13 and A15 are displayed. To further test whether the aneuploid strains described in *(26)* are karyotypically unstable, we isolated single colonies of different sizes from strains A13 and A15 and analyzed their karyotype via CGH. The karyotype of strain A13 was described in *(26)* as 1N + I, II, VIII, XI, XIII. A small A13 colony exhibited the reported 1N + I, II, VIII, XI, XIII karyotype. A colony of medium size had lost the additional copies of chromosomes XI and XIII and cells of the large colony had lost all additional chromosomes except for chromosome I. **(B)** The analysis in (A) was repeated for strain A15. While a small colony displayed the reported karyotype of 1N + II, III, VII, IX, XI, XII, cells from the medium and large colonies had lost the extra copies of chromosomes III, VII, IX, and XII but had gained a copy of chromosome X. We conclude that many strains described in *(26)* display significant karyotypic variation.

Supplemental Table S1. Mutation frequencies at *CAN1*

Strain	Basepair substitutions	Frameshifts	Complex Events	Transitions	Transversions	Insertions	Deletions
Wild-type	61.7% (82/133)	35.3% (47/133)	3.0% (4/133)	37.8% (31/82)	62.2% (51/82)	12.8% (6/47)	87.2% (41/47)
All aneuploids	59.4% (240/404)	34.9% (141/404)	**5.7% (23/404)****	36.7% (88/240)	63.3% (152/240)	10.6% (15/141)	89.4% (126/141)
Aneuploid mutators†	57.1% (89/156)	35.3% (55/156)	**7.7% (12/156)****	42.7% (38/89)	57.3% (51/89)	12.7% (7/55)	87.3% (48/55)
Disome I	58.3% (14/24)	29.2% (7/24)	12.5% (3/24)	21.4% (3/14)	78.6% (11/14)	28.6% (2/7)	71.4% (5/7)
Disome II	45.8% (11/24)	45.8% (11/24)	8.3% (2/24)	27.3% (3/11)	72.7% (8/11)	0.0% (0/11)	100% (11/11)
Disome IV	45.8% (11/24)	37.5% (9/24)	16.7% (4/24)	27.3% (3/11)	72.7% (8/11)	0.0% (0/9)	100% (9/9)
Disome VIII	50.0% (16/32)	43.8% (14/32)	6.3% (2/32)	25.0% (4/16)	75.0% (12/16)	21.4% (3/14)	78.6% (11/14)
Disome IX	67.1% (53/79)	30.4% (24/79)	2.5% (2/79)	35.8% (19/53)	64.2% (34/53)	12.5% (3/24)	87.5% (21/24)
Disome X	63.0% (46/73)	30.1% (22/73)	6.8% (5/73)	52.2% (24/46)	47.8% (22/46)	18.2% (4/22)	81.8% (18/22)
Disome XI	54.2% (13/24)	41.7% (10/24)	4.2% (1/24)	23.1% (3/13)	76.9% (10/13)	10.0% (1/10)	90.0% (9/10)
Disome XII	64.0% (16/25)	36.0% (9/25)	0.0% (0/25)	31.3% (5/16)	68.8% (11/16)	11.1% (1/9)	88.9% (8/9)
Disome XIII	54.2% (13/24)	45.8% (11/24)	0.0% (0/24)	15.4% (2/13)	84.6% (11/13)	9.1% (1/11)	90.9% (10/11)
Disome XIV	59.3% (16/27)	37.0% (10/27)	3.7% (1/27)	43.8% (7/16)	56.3% (9/16)	0.0% (0/10)	100% (10/10)
Disome XV	79.2% (19/24)	16.7% (4/24)	4.2% (1/24)	36.8% (7/19)	63.2% (12/19)	0.0% (0/4)	100% (4/4)
Disome XVI	50.0% (12/24)	41.7% (10/24)	8.3% (2/24)	66.7% (8/12)	33.3% (4/12)	0.0% (0/10)	100% (10/10)

** p<.005 (chi-square test)

† Aneuploid mutators are the combined results obtained with Dis. IV, VIII, X, and XIV

The ratios in parenthesis are the number of events observed and the total number of isolated sequenced of a particular strain.

Supplemental Table S2. Basepair substitutions in the coding strand at *CAN1*

Strain	Base Gained				Base Lost			
	A	**C**	**G**	**T**	**A**	**C**	**G**	**T**
Wild-type	45.1% (37/82)	15.9% (13/82)	7.3% (6/82)	31.7% (26/82)	4.9% (4/82)	41.5% (34/82)	45.1% (37/82)	8.5% (7/82)
All aneuploids	**55.4% (133/240)****	14.6% (35/240)	5.4% (13/240)	**24.6% (59/240)***	7.5% (18/240)	37.5% (90/240)	45.8% (110/240)	9.2% (22/240)
Aneuploid mutators†	53.9% (48/89)	19.1% (17/89)	5.6% (5/89)	**21.3% (19/89)***	10.1% (9/89)	32.6% (29/89)	47.2% (42/89)	10.1% (9/89)
Disome I	42.9% (6/14)	7.1% (1/14)	14.3% (2/14)	35.7% (5/14)	7.1% (1/14)	42.9% (6/14)	50.0% (7/14)	0.0% (0/14)
Disome II	63.6% (7/11)	27.3% (3/11)	0.0% (0/11)	9.1% (1/11)	0.0% (0/11)	36.4% (4/11)	45.5% (5/11)	18.2% (2/11)
Disome IV	45.5% (5/11)	45.5% (5/11)	0.0% (0/11)	9.1% (1/11)	0.0% (0/11)	45.5% (5/11)	45.5% (5/11)	9.1% (1/11)
Disome VIII	56.3% (9/16)	18.8% (3/16)	6.3% (1/16)	18.8% (3/16)	12.5% (2/16)	25.0% (4/16)	43.8% (7/16)	18.8% (3/16)
Disome IX	52.8% (28/53)	17.0% (9/53)	5.7% (3/53)	24.5% (13/53)	5.7% (3/53)	37.7% (20/53)	49.1% (26/53)	7.5% (4/53)
Disome X	52.2% (24/46)	13.0% (6/46)	6.5% (3/46)	28.3% (13/46)	13.0% (6/46)	30.4% (14/46)	45.7% (21/46)	10.9% (5/46)
Disome XI	53.8% (7/13)	15.4% (2/13)	0.0% (0/13)	30.8% (4/13)	7.7% (1/13)	46.2% (6/13)	38.5% (5/13)	7.7% (1/13)
Disome XII	50.0% (8/16)	6.3% (1/16)	0.0% (0/16)	43.8% (7/16)	6.3% (1/16)	56.3% (9/16)	31.3% (5/16)	6.3% (1/16)
Disome XIII	76.9% (10/13)	7.7% (1/13)	0.0% (0/13)	15.4% (2/13)	7.7% (1/13)	46.2% (6/13)	30.8% (4/13)	15.4% (2/13)
Disome XIV	62.5% (10/16)	18.8% (3/16)	6.3% (1/16)	12.5% (2/16)	6.3% (1/16)	37.5% (6/16)	56.3% (9/16)	0.0% (0/16)
Disome XV	68.4% (13/19)	0.0% (0/19)	10.5% (2/19)	21.1% (4/19)	5.3% (1/19)	31.6% (6/19)	52.6% (10/19)	10.5% (2/19)
Disome XVI	50.0% (6/12)	8.3% (1/12)	8.3% (1/12)	33.3% (4/12)	8.3% (1/12)	33.3% (4/12)	50.0% (6/12)	8.3% (1/12)

* p<.05; ** p<.005 (chi-square test)

† Aneuploid mutators include Dis. IV, VIII, X, and XIV

The ratios in parenthesis are the number of events observed and the total number of isolates in which a basepair substitution was found.

Supplemental Table S3. Basepair substitution events in the coding strand of *CAN1*

Strain	AT→CG	AT→GC	AT→TA	CG→AT	CG→GC	CG→TA	GC→AT	GC→CG	GC→TA	TA→AT	TA→CG	TA→GC
Wild-type	1.2% (1/82)	1.2% (1/82)	2.4% (2/82)	23.2% (19/82)	2.4% (2/82)	15.9% (13/82)	18.3% (15/82)	13.4% (11/82)	13.4% (11/82)	3.7% (3/82)	1.2% (1/82)	3.7% (3/82)
All aneuploids	2.5% (6/240)	0.0% (0/240)	**5.0% (12/240)***	24.2% (58/240)	**4.6% (11/240)***	**8.8% (21/240)****	**25.4% (61/240)****	9.6% (23/240)	10.8% (26/240)	5.8% (14/240)	2.5% (6/240)	**0.8% (2/240)***
Aneuploid mutators†	**4.5% (4/89)***	0.0% (0/89)	5.6% (5/89)	18.0% (16/89)	4.5% (4/89)	10.1% (9/89)	**29.2% (26/89)***	12.4% (11/89)	**5.6% (5/89)***	6.7% (6/89)	2.2% (2/89)	1.1% (1/89)
Disome I	0.0% (0/14)	0.0% (0/14)	7.1% (1/14)	21.4% (3/14)	14.3% (2/14)	7.1% (1/14)	21.4% (3/14)	7.1% (1/14)	21.4% (3/14)	0.0% (0/14)	0.0% (0/14)	0.0% (0/14)
Disome II	0.0% (0/11)	0.0% (0/11)	0.0% (0/11)	36.4% (4/11)	0.0% (0/11)	0.0% (0/11)	18.2% (2/11)	18.2% (2/11)	9.1% (1/11)	9.1% (1/11)	9.1% (1/11)	0.0% (0/11)
Disome IV	0.0% (0/11)	0.0% (0/11)	0.0% (0/11)	36.4% (4/11)	0.0% (0/11)	9.1% (1/11)	9.1% (1/11)	36.4% (4/11)	0.0% (0/11)	0.0% (0/11)	9.1% (1/11)	0.0% (0/11)
Disome VIII	0.0% (0/16)	0.0% (0/16)	12.5% (2/16)	18.8% (3/16)	6.3% (1/16)	0.0% (0/16)	18.8% (3/16)	18.8% (3/16)	6.3% (1/16)	18.8% (3/16)	0.0% (0/16)	0.0% (0/16)
Disome IX	1.9% (1/53)	0.0% (0/53)	3.8% (2/53)	24.5% (13/53)	5.7% (3/53)	7.5% (4/53)	24.5% (13/53)	11.3% (6/53)	13.2% (7/53)	3.8% (2/53)	3.8% (2/53)	0.0% (0/53)
Disome X	6.5% (3/46)	0.0% (0/46)	6.5% (3/46)	10.9% (5/46)	4.3% (2/46)	15.2% (7/46)	34.8% (16/46)	4.3% (2/46)	6.5% (3/46)	6.5% (3/46)	2.2% (1/46)	2.2% (1/46)
Disome XI	7.7% (1/13)	0.0% (0/13)	0.0% (0/13)	38.5% (5/13)	0.0% (0/13)	7.7% (1/13)	15.4% (2/13)	0.0% (0/13)	23.1% (3/13)	0.0% (0/13)	7.7% (1/13)	0.0% (0/13)
Disome XII	0.0% (0/16)	0.0% (0/16)	6.3% (1/16)	31.3% (5/16)	0.0% (0/16)	25.0% (4/16)	12.5% (2/16)	6.3% (1/16)	12.5% (2/16)	6.3% (1/16)	0.0% (0/16)	0.0% (0/16)
Disome XIII	0.0% (0/13)	0.0% (0/13)	7.7% (1/13)	46.2% (6/13)	0.0% (0/13)	0.0% (0/13)	15.4% (2/13)	7.7% (1/13)	7.7% (1/13)	15.4% (2/13)	0.0% (0/13)	0.0% (0/13)
Disome XIV	6.3% (1/16)	0.0% (0/16)	0.0% (0/16)	25.0% (4/16)	6.3% (1/16)	6.3% (1/16)	37.5% (6/16)	12.5% (2/16)	6.3% (1/16)	0.0% (0/16)	0.0% (0/16)	0.0% (0/16)
Disome XV	0.0% (0/19)	0.0% (0/19)	5.3% (1/19)	21.1% (4/19)	10.5% (2/19)	0.0% (0/19)	36.8% (7/19)	0.0% (0/19)	15.8% (3/19)	10.5% (2/19)	0.0% (0/19)	0.0% (0/19)
Disome XVI	0.0% (0/12)	0.0% (0/12)	8.3% (1/12)	16.7% (2/12)	0.0% (0/12)	16.7% (2/12)	33.3% (4/12)	8.3% (1/12)	8.3% (1/12)	0.0% (0/12)	0.0% (0/12)	8.3% (1/12)

* p<.05; ** p<.005 (chi-square test)

† Aneuploid mutators include Dis. IV, VIII, X, and XIV

The ratios in parenthesis are the number of events observed and the total number of isolates in which a basepair substitution was found. The first letter in each pair of nucleotides corresponds to the coding strand of *CAN1*

Supplemental Table S4. Strand-independent summary of basepair substitution events at CAN1

Strain	AT→TA	AT→CG	AT→GC	CG→AT	CG→TA	CG→GC
Wild-type	6.1% (5/82)	4.9% (4/82)	2.4% (2/82)	36.6% (30/82)	34.1% (28/82)	15.9% (13/82)
All aneuploids	**10.8% (26/240)****	3.3% (8/240)	2.5% (6/240)	35.0% (84/240)	34.2% (82/240)	14.2% (34/240)
Aneuploid mutators†	**12.4% (11/89)***	5.6% (5/89)	2.2% (2/89)	**23.6% (21/89)***	39.3% (35/89)	16.9% (15/89)
Disome I	7.1% (1/14)	0.0% (0/14)	0.0% (0/14)	42.9% (6/14)	28.6% (4/14)	21.4% (3/14)
Disome II	9.1% (1/11)	0.0% (0/11)	9.1% (1/11)	45.5% (5/11)	18.2% (2/11)	18.2% (2/11)
Disome IV	0.0% (0/11)	0.0% (0/11)	9.1% (1/11)	36.4% (4/11)	18.2% (2/11)	36.4% (4/11)
Disome VIII	31.3% (5/16)	0.0% (0/16)	0.0% (0/16)	25.0% (4/16)	18.8% (3/16)	25.0% (4/16)
Disome IX	7.5% (4/53)	1.9% (1/53)	3.8% (2/53)	37.7% (20/53)	32.1% (17/53)	17.0% (9/53)
Disome X	13.0% (6/46)	8.7% (4/46)	2.2% (1/46)	17.4% (8/46)	50.0% (23/46)	8.7% (4/46)
Disome XI	0.0% (0/13)	7.7% (1/13)	7.7% (1/13)	61.5% (8/13)	23.1% (3/13)	0.0% (0/13)
Disome XII	12.5% (2/16)	0.0% (0/16)	0.0% (0/16)	43.8% (7/16)	37.5% (6/16)	6.3% (1/16)
Disome XIII	23.1% (3/13)	0.0% (0/13)	0.0% (0/13)	53.8% (7/13)	15.4% (2/13)	7.7% (1/13)
Disome XIV	0.0% (0/16)	6.3% (1/16)	0.0% (0/16)	31.3% (5/16)	43.8% (7/16)	18.8% (3/16)
Disome XV	15.8% (3/19)	0.0% (0/19)	0.0% (0/19)	36.8% (7/19)	36.8% (7/19)	10.5% (2/19)
Disome XVI	8.3% (1/12)	8.3% (1/12)	0.0% (0/12)	25.0% (3/12)	50.0% (6/12)	8.3% (1/12)

* p<.05; ** p<.005 (chi-square test)

† Aneuploid mutators include Dis. IV, VIII, X, and XIV

The ratios in parenthesis are the number of events observed and the total number of isolates in which a basepair substitution was found.

Supplemental Table S5. Genomic instability in disomic yeast strains

Strain	Fluctuation assays			Drug sensitivities							Other assays		
	Increased mutation rate?	Increased chromosome loss?	Increased mitotic recom.?	Benomyl	CPT	HU	MMS	UV	Bleo	Phleo	Increased Rad52-GFP foci?	Large-budded arrest in *rad52Δ* cells?	Synthetic enhancement of genotoxic sensitivity with loss of *REV3*?
Wild-type	-	-	-	-	-	-	-	-	-	-	-	-	-
Disome I	-	+	ND	+	-	+	-	+	-	-	ND	ND	ND
Disome II	-	-	+	-	+	+	+	-	-	-	ND	ND	ND
Disome IV	+	-	ND	+	+	+	+	+	+	+	+	ND	+
Disome V	+	+	+	-	+	+	+	+	+	+	+	+	+
Disome VIII	+	+	+	-	+	+	+	+	+	+	+	-	+
Disome IX	-	+	-	+	-	-	-	+	-	-	ND	ND	ND
Disome X	+	-	+	-	+	+	+	+	+	+	+	ND	-
Disome XI	-	+	-	+	+	+	+	+	+	+	+	+	+
Disome XII	-	+	+	+	-	+	-	+	+	+	ND	+	-
Disome XIII	-	+	-	+	-	+	+	-	+	+	ND	ND	+
Disome XIV	+	-	+	+	+	+	+	+	+	+	+	+	+
Disome XV	-	+	+	+	+	+	+	+	+	+	+	-	+
Disome XVI	-	+	-	-	-	-	-	+	+	-	ND	ND	ND

(+) The strain exhibits an increase in the indicated assay or displays sensitivity to the indicated treatment
(-) The strain does not exhibit an increase in the indicated assay or displays wild-type growth in response to the indicated treatment
(ND) Not determined

Supplemental Table S6. Yeast strains used for strain construction

Strain Number	Genotype
A2587	MATa, ade2-1, leu2-3, ura3, trp1-1, his3-11,15, can1-100, GAL, psi+
A2588	MATα, ade2-1, leu2-3, ura3, trp1-1, his3-11,15, can1-100, GAL, psi+
	Relevant Genotype
A5316	MATα, PDS1-3HA::LEU2
A8625	MATa, mcm21::KanMX6
A12399	MATα, rad52::TRP1
A20745	MATα, CAN1
A20813	MATα, YAC: yWSS1572 [URA3 TRP1]
A22363	MATα, intergenic region (181900-182000) between YFR016C and YFR017C::URA3
A23884	MATα, pSH91 [TRP1 polyGT(16.5)-URA3]
A24286	MATα, RAD52-GFP::TRP1
A24493	MATα, rev3::LEU2
A24694	MATa, ade1::HIS3, chl4::KanMX6
A24803	MATα, mad2::LEU2
A25519	MATa, rad51::KanMX6
A25588	MATα, CAN1, hxt13::URA
A26291	MATα, rad18::TRP1
A26460	MATα, ade2::URA3::ade2
A27234	MATα, RAD52-GFP::KanMX6
A27290	MATa, RAD52-GFP::HIS3
A27897	MATα, msh2::LEU2

Supplemental Table S7. Yeast strains used in this study

Strain Number	Disome	Relevant Genotype
A11311	-	MATa, ade1::HIS3, lys2::KanMX6
A12683	I	MATa, ade1::HIS3, ade1::KanMX6
A12685	II	MATa, lys2::HIS3, lys2::KanMX6
A12687	IV	MATa, trp1::HIS3, trp1::KanMX6
A12689	X	MATa, ura2::HIS3, ura2::KanMX6
A12693	XII	MATa, ade16::HIS3, ade16::KanMX6
A12695	XIII	MATa, ura5::HIS3, ura5::KanMX6
A12697	XV	MATa, leu9::HIS3, leu9::KanMX6
A12700	XVI	MATa, met12::HIS3, met12::KanMX6
A13628	VIII	MATa, intergenic region (119778-119573) between YHR006W and YHR007C::HIS3, intergenic region (119778-119573) between YHR006W and YHR007C::KanMX6
A13771	XI	MATa, intergenic region (430900-431000) between YKL006C-A and YKL006W::HIS3, intergenic region (430900-431000) between YKL006C-A and YKL006W::KanMX6
A13975	IX	MATa, intergenic region (341900-3420000) between YIL009W and YIL008W::HIS3, intergenic region (341900-342000) between YIL009W and YIL008W::KanMX6
A13979	XIV	MATa, intergenic region (622880-622980) between YNL005C and YNL004W::HIS3, intergenic region (622880-622980) between YNL005C and YNL004W::KanMX6
A14479	V	MATa, can1::HIS3, intergenic region (187520-187620) between YER015W and YER016W::KanMX6
A15533	VIII	MATa, intergenic region (119778-119573) between YHR006W and YHR007C::HIS3, intergenic region (119778-119573) between YHR006W and YHR007C::URA3
A15537	XI	MATa, intergenic region (430900-431000) between YKL006C-A and YKL006W::HIS3, intergenic region (430900-431000) between YKL006C-A and YKL006W::URA3
A15538	XII	MATa, ade16::URA3, ade16::HIS3
A15540	XIV	MATa, intergenic region (622880-622980) between YNL005C and YNL004W::HIS3, intergenic region (622880-622980) between YNL005C and YNL004W::URA3

A15542	XV	MATa, leu9::HIS3, leu9::URA3
A15544	XVI	MATa, met12::HIS3, met12::URA3
A15546	-	MATa, ade1::HIS3, lys2::URA3
A18344	2N	MATa/α, ade1::HIS3, lys2::URA3, intergenic region (187520-187620) between FAA2 and BIM1::KanMX
A18346	2N+V	MATa/α, can1::HIS3, intergenic region (187520-187620) between YER015W and YER016W::KanMX6, intergenic region (187520-187620) between YER015W and YER016W::URA3
A18347	2N+VIII	MATa/α, MATa, intergenic region (119778-119573) between YHR006W and YHR007C::HIS3, intergenic region (119778-119573) between YHR006W and YHR007C::KanMX6, intergenic region (119778-119573) between YHR006W and YHR007C::URA3
A18349	2N+XIV	MATa/α, intergenic region (622880-622980) between YNL005C and YNL004W::HIS3, intergenic region (622880-622980) between YNL005C and YNL004W::KanMX6, intergenic region (622880-622980) between YNL005C and YNL004W::URA3
A18350	2N+XV	MATa/α, leu9::HIS3, leu9::KanMX6, leu9::URA3
A19549	2N+XII	MATa/α, ade16::HIS3, ade16::KanMX6, ade16::URA3
A19616	VIII	MATa, intergenic region (119778-119573) between YHR006W and YHR007C::HIS3, intergenic region (119778-119573) between YHR006W and YHR007C::URA3, rad52::TRP1
A19618	XII	MATa, ade16::HIS3, ade16::URA3. rad52::TRP1
A19619	XIV	MATa, intergenic region (622880-622980) between YNL005C and YNL004W::HIS3, intergenic region (622880-622980) between YNL005C and YNL004W::URA3, rad52::TRP1
A19620	XV	MATa, leu9::HIS3, leu9::URA3, rad52::TRP1
A20814	-	MATa, ade1::HIS3, lys2::KanMX6, CAN1
A21598	-	MATa, rad51::KanMX6, ade1::HIS3
A21630	-	MATa, rad51::KanMX6, ade1::HIS3, CAN1
A21986	X	MATa, intergenic region (322250-322350) betweem NUP82 and BNA3::HIS3, intergenic region (322250-322350) betweem NUP82 and BNA3::KanMX6
A21987	XIII	MATa, intergenic region (309200-309300) between YMR017W and YMR018W::HIS3, intergenic region (309200-309300) between YMR017W and YMR018W::KanMX6

A22296	-	MATa, ade2-1, leu2-3, ura3, trp1, his3, can1-100, ade1::HIS3, lys2::KanMX6, PDS1-3HA::LEU2
A23744	-	MATa, ade1::HIS3, lys2::KanMX6, YAC: yWSS1572 [URA3 TRP1]
A23745	I	MATa, ade1::HIS3, ade1::KanMX6, YAC: yWSS1572 [URA3 TRP1]
A23747	V	MATa, can1::HIS3, intergenic region (187520-187620) between YER015W and YER016W::KanMX6, YAC: yWSS1572 [URA3 TRP1]
A23748	VIII	MATa, intergenic region (119778-119573) between YHR006W and YHR007C::HIS3, intergenic region (119778-119573) between YHR006W and YHR007C::KanMX6, YAC: yWSS1572 [URA3 TRP1]
A23749	IX	MATa, intergenic region (341900-3420000) between YIL009W and YIL008W::HIS3, intergenic region (341900-342000) between YIL009W and YIL008W::KanMX6, YAC: yWSS1572 [URA3 TRP1]
A23750	XI	MATa, intergenic region (430900-431000) between YKL006C-A and YKL006W::HIS3, intergenic region (430900-431000) between YKL006C-A and YKL006W::KanMX6, YAC: yWSS1572 [URA3 TRP1]
A23751	XII	MATa, ade16::HIS3, ade16::KanMX6, YAC: yWSS1572 [URA3 TRP1]
A23752	XIV	MATa, intergenic region (622880-622980) between YNL005C and YNL004W::HIS3, intergenic region (622880-622980) between YNL005C and YNL004W::KanMX6, YAC: yWSS1572 [URA3 TRP1]
A23753	XV	MATa, leu9::HIS3, leu9::KanMX6, YAC: yWSS1572 [URA3 TRP1]
A24251	-	MATa, ade1::HIS3, lys2::KanMX6, pSH91: [TRP1 polyGT(16.5)-URA3]
A24287	V	MATa, can1::HIS3, intergenic region (187520-187620) between YER015W and YER016W::KanMX6, pSH91: [TRP1 polyGT(16.5)-URA3]
A24288	VIII	MATa, intergenic region (119778-119573) between YHR006W and YHR007C::HIS3, intergenic region (119778-119573) between YHR006W and YHR007C::KanMX6, pSH91: [TRP1 polyGT(16.5)-URA3]
A24289	I	MATa, ade1::HIS3, ade1::KanMX6, pSH91: [TRP1 polyGT(16.5)-URA3]

A24290	XIV	MATa, intergenic region (622880-622980) between YNL005C and YNL004W::HIS3, intergenic region (622880-622980) between YNL005C and YNL004W::KanMX6, pSH91: [TRP1 polyGT(16.5)-URA3]
A24291	XV	MATa, leu9::HIS3, leu9::KanMX6, pSH91: [TRP1 polyGT(16.5)-URA3]
A24351	-	MATa, ade1::HIS3, ade16::KanMX6
A24352	-	MATa, ade1::HIS3, lys2::KanMX6, RAD52-GFP::TRP1
A24660	-	MATa, ade1::HIS3, mcm21::KanMX6, YAC: yWSS1572 [URA3 TRP1]
A24792	-	MATa, ade1::HIS3, chl4::KanMX6, YAC: yWSS1572 [URA3 TRP1]
A25328	I	MATa, ade1::HIS3, ade1::KanMX6, CAN1
A25329	II	MATa, lys2::HIS3, lys2::KanMX6, CAN1
A25330	IV	MATa, trp1::HIS3, trp1::KanMX6, CAN1
A25331	VIII	MATa, intergenic region (119778-119573) between YHR006W and YHR007C::HIS3, intergenic region (119778-119573) between YHR006W and YHR007C::KanMX6, CAN1
A25332	IX	MATa, intergenic region (341900-342000) between YIL009W and YIL008W::HIS3, intergenic region (341900-342000) between YIL009W and YIL008W::KanMX6, CAN1
A25333	X	MATa, ura2::HIS3, ura2::KanMX6, CAN1
A25334	XI	MATa, intergenic region (430900-431000) between YKL006C-A and YKL006W::HIS3, intergenic region (430900-431000) between YKL006C-A and YKL006W::KanMX6, CAN1
A25335	XII	MATa, ade16::HIS3, ade16::KanMX6, CAN1
A25336	XIII	MATa, intergenic region (309200-309300) between YMR017W and YMR018W::HIS3, intergenic region (309200-309300) between YMR017W and YMR018W::KanMX6, CAN1
A25337	XIV	MATa, intergenic region (622880-622980) between YNL005C and YNL004W::HIS3, intergenic region (622880-622980) between YNL005C and YNL004W::KanMX6, CAN1
A25338	XV	MATa, leu9::HIS3, leu9::KanMX6, CAN1
A25339	XVI	MATa, met12::HIS3, met12::KanMX6, CAN1

A25340	IV	MATa, trp1::HIS3, trp1::KanMX6, YAC: yWSS1572 [URA3 TRP1]
A25341	XIII	MATa, intergenic region (309200-309300) between YMR017W and YMR018W::HIS3, intergenic region (309200-309300) between YMR017W and YMR018W::KanMX6, YAC: yWSS1572 [URA3 TRP1]
A25342	VIII	MATa, intergenic region (119778-119573) between YHR006W and YHR007C::HIS3, intergenic region (119778-119573) between YHR006W and YHR007C::KanMX6, RAD52-GFP::TRP1
A25343	X	MATa, ura2::HIS3, ura2::KanMX6, RAD52-GFP::TRP1
A25344	XIV	MATa, intergenic region (622880-622980) between YNL005C and YNL004W::HIS3, intergenic region (622880-622980) between YNL005C and YNL004W::KanMX6, RAD52-GFP::TRP1
A25345	XV	MATa, leu9::HIS3, leu9::KanMX6, RAD52-GFP::TRP1
A25360	-	MATa, ade1::HIS3, lys2::KanMX6, CAN1, rev3::LEU2
A25391	-	MATa, ade1::HIS3, lys2::KanMX6, rev3::LEU2
A25392	IV	MATa, trp1::HIS3, trp1::KanMX6, rev3::LEU2
A25393	VIII	MATa, intergenic region (119778-119573) between YHR006W and YHR007C::HIS3, intergenic region (119778-119573) between YHR006W and YHR007C::KanMX6, rev3::LEU2
A25394	X	MATa, ura2::HIS3, ura2::KanMX6, rev3::LEU2
A25395	XI	MATa, intergenic region (430900-431000) between YKL006C-A and YKL006W::HIS3, intergenic region (430900-431000) between YKL006C-A and YKL006W::KanMX6, rev3::LEU2
A25396	XIV	MATa, intergenic region (622880-622980) between YNL005C and YNL004W::HIS3, intergenic region (622880-622980) between YNL005C and YNL004W::KanMX6, rev3::LEU2
A25397	XV	MATa, leu9::HIS3, leu9::KanMX6, rev3::LEU2
A25413	V	MATa, can1::HIS3, intergenic region (187520-187620) between YER015W and YER016W::KanMX6, PDS1-3HA::LEU2
A25414	VIII	MATa, intergenic region (119778-119573) between YHR006W and YHR007C::HIS3, intergenic region (119778-119573) between YHR006W and YHR007C::KanMX6, PDS1-3HA::LEU2

A25415	XI	MATa, intergenic region (430900-431000) between YKL006C-A and YKL006W::HIS3, intergenic region (430900-431000) between YKL006C-A and YKL006W::KanMX6, PDS1-3HA::LEU2
A25416	XVI	MATa, met12::HIS3, met12::KanMX6, PDS1-3HA::LEU2
A25417	IV	MATa, trp1::HIS3, trp1::KanMX6, CAN1, rev3::LEU2
A25418	VIII	MATa, intergenic region (119778-119573) between YHR006W and YHR007C::HIS3, intergenic region (119778-119573) between YHR006W and YHR007C::KanMX6, CAN1, rev3::LEU2
A25419	X	MATa, ura2::HIS3, ura2::KanMX6, CAN1, rev3::LEU2
A25420	XIV	MATa, intergenic region (622880-622980) between YNL005C and YNL004W::HIS3, intergenic region (622880-622980) between YNL005C and YNL004W::KanMX6, CAN1, rev3::LEU2
A25421	XI	MATa, intergenic region (430900-431000) between YKL006C-A and YKL006W::HIS3, intergenic region (430900-431000) between YKL006C-A and YKL006W::KanMX6, RAD52-GFP::TRP1
A25582	-	MATa, ade1::HIS3, lys2::KanMX6, mad2::LEU2, YAC: yWSS1572 [URA3 TRP1]
A25583	VIII	MATa, intergenic region (119778-119573) between YHR006W and YHR007C::HIS3, intergenic region (119778-119573) between YHR006W and YHR007C::KanMX6, mad2::LEU2, YAC: yWSS1572 [URA3 TRP1]
A25584	XI	MATa, intergenic region (430900-431000) between YKL006C-A and YKL006W::HIS3, intergenic region (430900-431000) between YKL006C-A and YKL006W::KanMX6, mad2::LEU2, YAC: yWSS1572 [URA3 TRP1]
A25585	XII	MATa, ade16::HIS3, ade16::KanMX6, mad2::LEU2, YAC: yWSS1572 [URA3 TRP1]
A25586	XIII	MATa, intergenic region (309200-309300) between YMR017W and YMR018W::HIS3, intergenic region (309200-309300) between YMR017W and YMR018W::KanMX6, RAD52-GFP::TRP1
A25587	X	MATa, intergenic region (322250-322350) betweem NUP82 and BNA3::HIS3, intergenic region (322250-322350) betweem NUP82 and BNA3::KanMX6, YAC: yWSS1572 [URA3 TRP1]
A25589	-	MATa, ade1::HIS3, lys2::KanMX6, hxt13::URA3

A25590	IV	MATa, trp1::HIS3, trp1::KanMX6, hxt13::URA3
A25591	VIII	MATa, intergenic region (119778-119573) between YHR006W and YHR007C::HIS3, intergenic region (119778-119573) between YHR006W and YHR007C::KanMX6, hxt13::URA3
A25592	X	MATa, intergenic region (322250-322350) betweem NUP82 and BNA3::HIS3, intergenic region (322250-322350) betweem NUP82 and BNA3::KanMX6, hxt13::URA3
A25593	XIV	MATa, intergenic region (622880-622980) between YNL005C and YNL004W::HIS3, intergenic region (622880-622980) between YNL005C and YNL004W::KanMX6, hxt13::URA3
A25627	XVI	MATa, met12::HIS3, met12::KanMX6, YAC: yWSS1572 [URA3 TRP1]
A25827	II	MATa, lys2::HIS3, lys2::KanMX6, YAC: yWSS1572 [URA3 TRP1]
A26459	-	MATa, lys2::KanMX6, lys9::HIS3
A26461	-	MATa, lys2::KanMX6, lys9::HIS3, ade2::URA3::ade2
A26462	II	MATa, lys2::HIS3, lys2::KanMX6, ade2::URA3::ade2
A26463	V	MATa, can1::HIS3, intergenic region (187520-187620) between YER015W and YER016W::KanMX6, ade2::URA3::ade2
A26464	VIII	MATa, intergenic region (119778-119573) between YHR006W and YHR007C::HIS3, intergenic region (119778-119573) between YHR006W and YHR007C::KanMX6, ade2::URA3::ade2
A26465	IX	MATa, intergenic region (341900-342000) between YIL009W and YIL008W::HIS3, intergenic region (341900-342000) between YIL009W and YIL008W::KanMX6, ade2::URA3::ade2
A26466	X	MATa, intergenic region (322250-322350) betweem NUP82 and BNA3::HIS3, intergenic region (322250-322350) betweem NUP82 and BNA3::KanMX6, ade2::URA3::ade2
A26467	XI	MATa, intergenic region (430900-431000) between YKL006C-A and YKL006W::HIS3, intergenic region (430900-431000) between YKL006C-A and YKL006W::KanMX6, ade2::URA3::ade2
A26468	XII	MATa, ade16::HIS3, ade16::KanMX6, ade2::URA3::ade2

A26469	XIII	MATa, intergenic region (309200-309300) between YMR017W and YMR018W::HIS3, intergenic region (309200-309300) between YMR017W and YMR018W::KanMX6, ade2::URA3::ade2
A26470	XIV	MATa, intergenic region (622880-622980) between YNL005C and YNL004W::HIS3, intergenic region (622880-622980) between YNL005C and YNL004W::KanMX6, ade2::URA3::ade2
A26471	XV	MATa, leu9::HIS3, leu9::KanMX6, ade2::URA3::ade2
A26472	XVI	MATa, met12::HIS3, met12::KanMX6, ade2::URA3::ade2
A26473	-	MATa, lys2::KanMX6, lys9::HIS3, ade2::URA3::ade2, rad18::TRP1
A26475	-	MATa, lys2::KanMX6, lys9::HIS3, ade2::URA3::ade2, rad52::TRP1
A26498	IV	MATa, trp1::HIS3, trp1::KanMX6, pSH91: [TRP1 polyGT(16.5)-URA3]
A26499	IX	MATa, intergenic region (341900-342000) between YIL009W and YIL008W::HIS3, intergenic region (341900-342000) between YIL009W and YIL008W::KanMX6, pSH91: [TRP1 polyGT(16.5)-URA3]
A26500	XI	MATa, intergenic region (430900-431000) between YKL006C-A and YKL006W::HIS3, intergenic region (430900-431000) between YKL006C-A and YKL006W::KanMX6, pSH91: [TRP1 polyGT(16.5)-URA3]
A26501	XVI	MATa, met12::HIS3, met12::KanMX6, pSH91: [TRP1 polyGT(16.5)-URA3]
A26504	-	MATa, ade1::HIS3, lys2::URA3, rad52::TRP1
A26532	IV	MATa, trp1::HIS3, trp1::KanMX6, Rad52-GFP::TRP1
A26533	V	MATa, can1::HIS3, intergenic region (187520-187620) between YER015W and YER016W::KanMX6, Rad52-GFP::TRP1
A26549	XV	MATa, leu9::HIS3, leu9::KanMX6, mad2::LEU2, YAC: yWSS1572 [URA3 TRP1]
A26628	XV	MATa, leu9::HIS3, leu9::KanMX6, PDS1-3HA::LEU2
A26629	V	MATa, can1::HIS3, intergenic region (187520-187620) between YER015W and YER016W::KanMX6, rev3::LEU2
A26630	XII	MATa, ade16::HIS3, ade16::KanMX6, rev3::LEU2

A26631	XIII	MATa, intergenic region (309200-309300) between YMR017W and YMR018W::HIS3, intergenic region (309200-309300) between YMR017W and YMR018W::KanMX6, rev3::LEU2
A26640	XVI	MATa, met12::HIS3, met12::KanMX6, mad2::LEU2, YAC: yWSS1572 [URA3 TRP1]
A26703	-	MATa, ade1::HIS3, lys2::KanMX6, PDS1-3HA::LEU2
A26704	XI	MATa, intergenic region (430900-431000) between YKL006C-A and YKL006W::HIS3, intergenic region (430900-431000) between YKL006C-A and YKL006W::KanMX6, PDS1-3HA::LEU2, mad2::LEU2
A26705	XVI	MATa, met12::HIS3, met12::KanMX6, PDS1-3HA::LEU2, mad2::LEU2
A26708	V	MATa, can1::HIS3, intergenic region (187520-187620) between YER015W and YER016W::KanMX6, PDS1-3HA::LEU2, mad2::LEU2
A26709	VIII	MATa, intergenic region (119778-119573) between YHR006W and YHR007C::HIS3, intergenic region (119778-119573) between YHR006W and YHR007C::KanMX6, PDS1-3HA::LEU2, mad2::LEU2
A26717	-	MATa, ade1::HIS3, lys2::KanMX6, intergenic region (181900-182000) between YFR016C and YFR017C::URA3
A26718	V	MATa, can1::HIS3, intergenic region (187520-187620) between YER015W and YER016W::KanMX6, intergenic region (181900-182000) between YFR016C and YFR017C::URA3
A27091	XI	MATa, intergenic region (430900-431000) between YKL006C-A and YKL006W::HIS3, intergenic region (430900-431000) between YKL006C-A and YKL006W::URA3, rad52::TRP1
A27223	V	MATa, can1::HIS3, intergenic region (187520-187620) between YER015W and YER016W::URA3
A27889	2N	MATa/α, ade1::HIS3, lys2::KanMX6, lys2::LEU2, YAC: yWSS1572 [URA3 TRP1]
A27890	2N+XI	MATa/α, intergenic region (430900-431000) between YKL006C-A and YKL006W::HIS3, intergenic region (430900-431000) between YKL006C-A and YKL006W::KanMX6, intergenic region (430900-431000) between YKL006C-A and YKL006W::LEU2, YAC: yWSS1572 [URA3 TRP1]

A27891	2N+XIII	MATa/α, intergenic region (309200-309300) between YMR017W and YMR018W::HIS3, intergenic region (309200-309300) between YMR017W and YMR018W::KanMX6, intergenic region (309200-309300) between YMR017W and YMR018W::LEU2, YAC: yWSS1572 [URA3 TRP1]
A27892	2N+XV	MATa/α, leu9::KanMX6, leu9::HIS3, leu9::LEU2, YAC: yWSS1572 [URA3 TRP1]
A27898	-	MATa, ade1::HIS3, lys2::KanMX6, msh2::LEU2, CAN1
A27997	2N	MATa/α, RAD52-GFP::HIS3, RAD52-GFP::KanMX6
A28064	V	MATa, can1::HIS3, intergenic region (187520-187620) between YER015W and YER016W::URA3, rad52::TRP1
A28502	3N	MATa/a/α, RAD52-GFP::TRP1, RAD52-GFP::HIS3, RAD52-GFP::KanMX6

Supplemental Table S8. Euploid strains containing YACs used in this study

Strain number	YAC number	Approximate Size (kb)	Source of DNA	Previous nomenclature	Source
A17392	YAC-2	850	Human Chr. Y	yOX39	Foote et al.
A17393	YAC-3	670	Human Chr. Y	yOX32	Foote et al.
A17394	YAC-4	620	Human Chr. Y	yOX41	Foote et al.
A17395	YAC-5	630	Human Chr. Y	yOX21	Foote et al.
A17396	YAC-6	580	Human Chr. Y	yOX2190	Foote et al.
A23744	YAC-7	340	Human Chr. VII	yWSS1572	Huang et al.
		Relevant Genotype			
A26980	YAC-2	MATa, ade1::HIS3, lys2::KanMX6, CAN1			
A26981	YAC-3	MATa, ade1::HIS3, lys2::KanMX6, CAN1			
A26985	YAC-2	MATa, ade1::HIS3, lys2::KanMX6, RAD52-GFP::TRP1			
A26986	YAC-3	MATa, ade1::HIS3, lys2::KanMX6, RAD52-GFP::TRP1			
A27667	YAC-4	MATa, ade1::HIS3, lys2::KanMX6, RAD52-GFP::TRP1			
A27683	YAC-4	MATa, ade1::HIS3, lys2::KanMX6, CAN1			

Supplemental Table S9. *Schizosaccharomyces pombe* strains used in this study

Strain Number	Karyotype	Relevant Genotype
HM123	1N	h- leu1
P219	Dis. III	h- leu1 ade6-M210/ade6-M216
P321	1N	h+ rad22-GFPvenus
P322	2N	h-/h- leu1/leu1 rad22-GFPvenus/rad22-GFPvenus
P523	1N	h+ leu1 rhp51::KanMX6

Text References and Notes

1. E. M. Torres, B. R. Williams, A. Amon, Aneuploidy: Cells losing their balance. *Genetics* **179**, 737 (2008). doi:10.1534/genetics.108.090878 Medline

2. B. A. Weaver, D. W. Cleveland, Does aneuploidy cause cancer? *Curr. Opin. Cell Biol.* **18**, 658 (2006). doi:10.1016/j.ceb.2006.10.002 Medline

3. M. A. Matzke, M. F. Mette, T. Kanno, A. J. M. Matzke, Does the intrinsic instability of aneuploid genomes have a causal role in cancer? *Trends Genet.* **19**, 253 (2003). doi:10.1016/S0168-9525(03)00057-X Medline

4. E. M. Torres *et al*., Effects of aneuploidy on cellular physiology and cell division in haploid yeast. *Science* **317**, 916 (2007). doi:10.1126/science.1142210 Medline

5. E. M. Torres *et al*., Identification of aneuploidy-tolerating mutations. *Cell* **143**, 71 (2010). doi:10.1016/j.cell.2010.08.038 Medline

6. A. Musacchio, E. D. Salmon, The spindle-assembly checkpoint in space and time. *Nat. Rev. Mol. Cell Biol.* **8**, 379 (2007). doi:10.1038/nrm2163 Medline

7. Materials and methods are available as supporting material on *Science* Online.

8. B. D. Harfe, S. Jinks-Robertson, DNA polymerase zeta introduces multiple mutations when bypassing spontaneous DNA damage in *Saccharomyces cerevisiae*. *Mol. Cell* **6**, 1491 (2000). doi:10.1016/S1097-2765(00)00145-3 Medline

9. N. Pavelka *et al*., Aneuploidy confers quantitative proteome changes and phenotypic variation in budding yeast. *Nature* **468**, 321 (2010). doi:10.1038/nature09529 Medline

10. A. J. Rattray, B. K. Shafer, C. B. McGill, J. N. Strathern, The roles of REV3 and RAD57 in double-strand-break-repair-induced mutagenesis of *Saccharomyces cerevisiae*. *Genetics* **162**, 1063 (2002). Medline

11. J. Chen, J. Stubbe, Bleomycins: Towards better therapeutics. *Nat. Rev. Cancer* **5**, 102 (2005). doi:10.1038/nrc1547 Medline

12. M. Lisby, R. Rothstein, U. H. Mortensen, Rad52 forms DNA repair and recombination centers during S phase. *Proc. Natl. Acad. Sci. U.S.A.* **98**, 8276 (2001). doi:10.1073/pnas.121006298 Medline

13. F. Pâques, J. E. Haber, Multiple pathways of recombination induced by double-strand breaks in *Saccharomyces cerevisiae*. *Microbiol. Mol. Biol. Rev.* **63**, 349 (1999). Medline

14. O. Niwa, Y. Tange, A. Kurabayashi, Growth arrest and chromosome instability in aneuploid yeast. *Yeast* **23**, 937 (2006). doi:10.1002/yea.1411 Medline

15. P. Meister *et al*., Nuclear factories for signalling and repairing DNA double strand breaks in living fission yeast. *Nucleic Acids Res.* **31**, 5064 (2003). doi:10.1093/nar/gkg719 Medline

16. J. Takeda *et al*., Radiation induction of delayed recombination in *Schizosaccharomyces pombe*. *DNA Repair (Amst.)* **7**, 1250 (2008). doi:10.1016/j.dnarep.2008.04.006 Medline

17. J. St. Charles, M. L. Hamilton, T. D. Petes, Meiotic chromosome segregation in triploid strains of *Saccharomyces cerevisiae*. *Genetics* **186**, 537 (2010). Medline doi:10.1534/genetics.110.121533

18. A. T. Natarajan, in *DNA Repair and Human Disease*, A. S. Balajee, Ed. (Landes Bioscience and Springer Science+Business Media, New York, 2006), pp. 61–66.

19. P. Duesberg, C. Rausch, D. Rasnick, R. Hehlmann, Genetic instability of cancer cells is proportional to their degree of aneuploidy. *Proc. Natl. Acad. Sci. U.S.A.* **95**, 13692 (1998). doi:10.1073/pnas.95.23.13692 Medline

20. S. L. Thompson, D. A. Compton, Proliferation of aneuploid human cells is limited by a p53-dependent mechanism. *J. Cell Biol.* **188**, 369 (2010). doi:10.1083/jcb.200905057 Medline

21. C. Lengauer, K. W. Kinzler, B. Vogelstein, Genetic instabilities in human cancers. *Nature* **396**, 643 (1998). doi:10.1038/25292 Medline

22. P. D. Sniegowski, P. J. Gerrish, R. E. Lenski, Evolution of high mutation rates in experimental populations of *E. coli*. *Nature* **387**, 703 (1997). doi:10.1038/42701 Medline

23. A. C. Shaver *et al*., Fitness evolution and the rise of mutator alleles in experimental *Escherichia coli* populations. *Genetics* **162**, 557 (2002). Medline

24. B. R. Williams *et al*., Aneuploidy affects proliferation and spontaneous immortalization in mammalian cells. *Science* **322**, 703 (2008). doi:10.1126/science.1160058 Medline

Supporting References and Notes

1. E. M. Torres *et al*., Effects of aneuploidy on cellular physiology and cell division in haploid yeast. *Science* **317**, 916 (2007). doi:10.1126/science.1142210 Medline

2. M. P. Rossmann, W. Luo, O. Tsaponina, A. Chabes, B. Stillman, A common telomeric gene silencing assay is affected by nucleotide metabolism. *Mol. Cell* **42**, 127 (2011). doi:10.1016/j.molcel.2011.03.007 Medline

3. B. S. Strauss, The ‘A rule’ of mutagen specificity: A consequence of DNA polymerase bypass of non-instructional lesions? *Bioessays* **13**, 79 (1991). doi:10.1002/bies.950130206 Medline

4. M. Bellaoui *et al*., Elg1 forms an alternative RFC complex important for DNA replication and genome integrity. *EMBO J.* **22**, 4304 (2003). doi:10.1093/emboj/cdg406 Medline

5. R. Driscoll, A. Hudson, S. P. Jackson, Yeast Rtt109 promotes genome stability by acetylating histone H3 on lysine 56. *Science* **315**, 649 (2007). doi:10.1126/science.1135862 Medline

6. H. W. Mankouri, H.-P. Ngo, I. D. Hickson, Esc2 and Sgs1 act in functionally distinct branches of the homologous recombination repair pathway in *Saccharomyces cerevisiae*. *Mol. Biol. Cell* **20**, 1683 (2009). doi:10.1091/mbc.E08-08-0877 Medline

7. W.-C. Au, M. J. Crisp, S. Z. DeLuca, O. J. Rando, M. A. Basrai, Altered dosage and mislocalization of histone H3 and Cse4p lead to chromosome loss in *Saccharomyces cerevisiae*. *Genetics* **179**, 263 (2008). doi:10.1534/genetics.108.088518 Medline

8. H. J. Chial, T. H. Giddings, Jr., E. A. Siewert, M. A. Hoyt, M. Winey, Altered dosage of the *Saccharomyces cerevisiae* spindle pole body duplication gene, NDC1, leads to

aneuploidy and polyploidy. *Proc. Natl. Acad. Sci. U.S.A.* **96**, 10200 (1999). doi:10.1073/pnas.96.18.10200 Medline

9. D. Meeks-Wagner, L. H. Hartwell, Normal stoichiometry of histone dimer sets is necessary for high fidelity of mitotic chromosome transmission. *Cell* **44**, 43 (1986). doi:10.1016/0092-8674(86)90483-6 Medline

10. E. M. Torres *et al*., Identification of aneuploidy-tolerating mutations. *Cell* **143**, 71 (2010). doi:10.1016/j.cell.2010.08.038 Medline

11. M. S. Longtine *et al*., Additional modules for versatile and economical PCR-based gene deletion and modification in *Saccharomyces cerevisiae*. *Yeast* **14**, 953 (1998). doi:10.1002/(SICI)1097-0061(199807)14:10<953::AID-YEA293>3.0.CO;2-U Medline

12. D. Huang, D. Koshland, Chromosome integrity in *Saccharomyces cerevisiae*: The interplay of DNA replication initiation factors, elongation factors, and origins. *Genes Dev.* **17**, 1741 (2003). doi:10.1101/gad.1089203 Medline

13. S. Foote, D. Vollrath, A. Hilton, D. C. Page, The human Y chromosome: Overlapping DNA clones spanning the euchromatic region. *Science* **258**, 60 (1992). doi:10.1126/science.1359640 Medline

14. G. M. Dani, V. A. Zakian, Mitotic and meiotic stability of linear plasmids in yeast. *Proc. Natl. Acad. Sci. U.S.A.* **80**, 3406 (1983). doi:10.1073/pnas.80.11.3406 Medline

15. J. V. Kilmartin, A. E. Adams, Structural rearrangements of tubulin and actin during the cell cycle of the yeast *Saccharomyces*. *J. Cell Biol.* **98**, 922 (1984). doi:10.1083/jcb.98.3.922 Medline

16. D. Lea, C. Coulson, The distribution of the numbers of mutants in bacterial populations. *J. Genet.* **49**, 264 (1949). doi:10.1007/BF02986080

17. B. M. Hall, C.-X. Ma, P. Liang, K. K. Singh, Fluctuation analysis CalculatOR: A web tool for the determination of mutation rate using Luria-Delbruck fluctuation analysis. *Bioinformatics* **25**, 1564 (2009). doi:10.1093/bioinformatics/btp253 Medline

18. S. Ito-Harashima, P. E. Hartzog, H. Sinha, J. H. McCusker, The tRNA-Tyr gene family of *Saccharomyces cerevisiae*: Agents of phenotypic variation and position effects on mutation frequency. *Genetics* **161**, 1395 (2002). Medline

19. P. Fiorentini, K. N. Huang, D. X. Tishkoff, R. D. Kolodner, L. S. Symington, Exonuclease I of *Saccharomyces cerevisiae* functions in mitotic recombination in vivo and in vitro. *Mol. Cell. Biol.* **17**, 2764 (1997). Medline

20. M. Strand, T. A. Prolla, R. M. Liskay, T. D. Petes, Destabilization of tracts of simple repetitive DNA in yeast by mutations affecting DNA mismatch repair. *Nature* **365**, 274 (1993). doi:10.1038/365274a0 Medline

21. C. S. Hoffman, F. Winston, A ten-minute DNA preparation from yeast efficiently releases autonomous plasmids for transformation of *Escherichia coli*. *Gene* **57**, 267 (1987). doi:10.1016/0378-1119(87)90131-4 Medline

22. G. I. Lang, A. W. Murray, Estimating the per-base-pair mutation rate in the yeast *Saccharomyces cerevisiae*. *Genetics* **178**, 67 (2008). doi:10.1534/genetics.107.071506 Medline

23. D. C. Schwartz, C. R. Cantor, Separation of yeast chromosome-sized DNAs by pulsed field gradient gel electrophoresis. *Cell* **37**, 67 (1984). doi:10.1016/0092-8674(84)90301-5 Medline

24. O. Niwa, M. Yanagida, Triploid meiosis and aneuploidy in *Schizosaccharomyces pombe*: An unstable aneuploid disomic for chromosome III. *Curr. Genet.* **9**, 463 (1985). doi:10.1007/BF00434051

25. O. Niwa, Y. Tange, A. Kurabayashi, Growth arrest and chromosome instability in aneuploid yeast. *Yeast* **23**, 937 (2006). doi:10.1002/yea.1411 Medline

26. N. Pavelka *et al*., Aneuploidy confers quantitative proteome changes and phenotypic variation in budding yeast. *Nature* **468**, 321 (2010). doi:10.1038/nature09529 Medline

Acknowledgements: We are grateful to Eduardo M. Torres for the data shown in Figs. S13 and S14.